Available online at www.sciencedirect.com
ScienceDirect
Geochimica et Cosmochimica Acta 74 (2010) 2142–2164
Geochimica et Cosmochimica Acta
www.elsevier.com/locate/gca

Mineralogical impact on organic nitrogen across a long-term soil chronosequence (0.3–4100 kyr)

Robert Mikutta [a,*], Klaus Kaiser [b], Nicole Dörr [a], Antje Vollmer [c], Oliver A. Chadwick [d], Jon Chorover [e], Marc G. Kramer [f], Georg Guggenberger [a]

[a] *Institute of Soil Science and Centre for Solid State Chemistry and New Materials (ZFM), Leibniz Universität Hannover, Germany*
[b] *Soil Sciences, Martin Luther University Halle-Wittenberg, Germany*
[c] *Berliner Elektronenspeicherring-Gesellschaft für Synchrotronstrahlung (BESSY), Germany*
[d] *Department of Geography, University of California, Santa Barbara, USA*
[e] *Department of Soil, Water and Environmental Science, University of Arizona, USA*
[f] *Earth and Planetary Sciences, University of California, Santa Cruz, USA*

Received 11 March 2009; accepted in revised form 5 January 2010; available online 13 January 2010

Abstract

Large portions of organic N (ON) in soil exist tightly associated with minerals. Mineral effects on the type of interactions, chemical composition, and stability of ON, however, are poorly understood. We investigated mineral-associated ON along a Hawaiian soil chronosequence (0.3–4100 kyr) formed in basaltic tephra under comparable climatic, topographic, and vegetation conditions. Mineral–organic associations were separated according to density ($\rho > 1.6$ g/cm^3), characterized by X-ray photoelectron spectroscopy (XPS), X-ray absorption near edge fine structure (NEXAFS) and analyzed for amino acid enantiomers and amino sugars. The ^{14}C activity of mineral-bound OC was estimated by accelerator mass spectrometry. The close OC–ON relationship ($r = 0.96$) and XPS results suggest that ON exists incorporated in bulk mineral-bound OM and likely becomes associated with minerals as part of sorbing OM. The youngest site (0.3 kyr), with soils mainly composed of primary minerals (olivine, pyroxene, feldspar) and with little ON, contained the largest proportion of hydrolyzable amino sugars and amino acids but with a small share of acidic amino acids (aspartic acid, glutamic acid). In soils of the intermediate weathering stage (20–400 kyr), where poorly crystalline minerals and metal(hydroxide)–organic precipitates prevail, more mineral-associated ON was present, containing a smaller proportion of hydrolyzable amino sugars and amino acids due to the preferential accumulation of other OM components such as lignin-derived phenols. Acidic amino acids were more abundant, reflecting the strong association of acidic organic components with metal(hydroxide)–organic precipitates and variable-charge minerals. In the final weathering stage (1400–4100 kyr) with well-crystalline secondary Fe and Al (hydr)oxides and kaolin minerals, mineral–organic associations held less ON and were, relative to lignin phenols, depleted in hydrolyzable amino sugars and amino acids, particularly in acidic amino acids. XPS and NEXAFS analyses showed that the majority (59–78%) of the mineral-associated ON is peptide N while 18–34% was aromatic N. Amino sugar ratios and D-alanine suggest that mineral-associated ON comprises a significant portion of bacterial residues, particularly in the subsoil. With increasing ^{14}C age, a larger portion of peptide N was non-hydrolyzable, suggesting the accumulation of refractory compounds with time. The constant D/L ratios of lysine in topsoils indicate fresh proteinous material, likely due to continuous sorption of or exchange with fresh N-containing compounds. The ^{14}C and the D/L signature revealed a longer turnover of proteinous components strongly bound to minerals (not NaOH–NaF-extractable). This study provides evidence that interactions with minerals are important in the transformation and stabilization of soil ON. Mineral-associated ON in topsoils seems actively involved in the N cycling of the study ecosystems, accentuating N limitation at the 0.3-kyr site but increasing N availability at older sites.

* Corresponding author. Tel.: +49 511 762 2622.
E-mail address: mikutta@ifbk.uni-hannover.de (R. Mikutta).

0016-7037/$ - see front matter © 2010 Elsevier Ltd. All rights reserved.
doi:10.1016/j.gca.2010.01.006

1. INTRODUCTION

Most biosphere nitrogen (N) exists in soils (10.5×10^{16} g; Paul and Clark, 1996), with organic matter (OM) being the main N reservoir. While simple organic N (ON) forms like amino acids and amino sugars become mineralized rapidly (van Hees et al., 2005), a portion of ON turns over slowly, thus is, at least temporarily, taken out of the biological cycle (Gleixner et al., 2002; Amelung et al., 2006). Nitrogenous compounds are assumed to be stabilized, i.e., rendered less bioavailable, by interactions with other organic matter. The suggested mechanisms include encapsulation of proteins into resistant aliphatic polymers, chemical incorporation of peptides and proteins into or their association with complex biomolecules as well as reactions of proteins with reducing sugars (Maillard reaction), polyphenols, quinones, and tannins (Nguyen and Harvey, 2001; Espeland and Wetzel, 2001; Fan et al., 2004; Knicker, 2004; Hsu and Hatcher, 2005).

Since interactions with minerals stabilize OM against biological decay (Kalbitz et al., 2005; Mikutta et al., 2007), mineral–organic interactions might also impact the cycling of N in soil. Densiometric fractionation of soils revealed that a large portion of N is associated with minerals (Rovira and Vallejo, 2003; Sollins et al., 2006). Proteins and ribonucleic acids show a large affinity for 1:1 and 1:2 clay minerals (Safari Sinegani et al., 2005; Levy-Booth et al., 2007; Fu et al., 2008) and Fe oxyhydroxides selectively retain N-rich constituents of bacterial exopolymeric substances (Omoike and Chorover, 2006). Sorption selectivity can be the result of the charge properties of nitrogenous compounds. Basic amino acids are typically enriched in environments with negatively charged aluminosilicate minerals (Keil et al., 1998; Aufdenkampe et al., 2001) while sorption to metal oxides is selective for acidic amino acids (Matrajt and Blanot, 2004).

Based on these findings, we hypothesize that patterns of ON accumulation and stabilization in soil change with the mineral assemblage. Minerals may alter the N bioavailability and interfere with the N uptake by plants and microorganisms. The magnitude of this interference and the stability of mineral-associated ON likely depend on the properties of the soil mineral phase. Examining ON–mineral relationships is therefore a key to understand soil N cycling and the possible feedbacks to ecosystem productivity.

In a previous study, we investigated the mineral–organic associations across the Hawaiian substrate gradient, covering parent material ages from 0.3 to 4100 kyr (Mikutta et al., 2009 and Table 1). Soil mineral composition as well as the chemical composition of mineral-bound OM changed along the weathering gradient. The youngest, 0.3-kyr site (stage I), comprising mainly primary minerals (olivine, pyroxene, feldspar), contained little while the 20–400-kyr sites (stage II), with prevailing poorly crystalline minerals and metal (hydroxide)–organic coprecipitates, had most mineral–associated OM. Mineral-bound OM decreased in the oldest soils (1400 and 4100 kyr; stage III) that are dominated by crystalline secondary clay and oxide minerals. Non-cellulosic carbohydrates were more prominent at the youngest site while lignin-derived phenols were most concentrated between 20 and 400 kyr. This differential accumulation of OM and biomolecules suggests that the changing mineral composition may also impact the accumulation and transformation of ON.

We, therefore, examined mineral–organic associations separated from soils of the Hawaiian weathering sequence for the chemical composition of ON using X-ray photoelectron spectroscopy (XPS) and near edge X-ray absorption fine structure (NEXAFS) spectroscopy. Since N-containing compounds such as proteins, chitin, and peptidoglycan constitute important fractions of soil ON (Amelung, 2003), we analyzed the molecular composition of hydrolyzable amino acids and amino sugars as proxies for biopolymeric N sources. The participation of proteins in biological cycles was deduced from the composition of hydrolyzable amino acid enantiomers (Brodowski et al., 2004; Amelung et al., 2006). Specifically, D-lysine was used to qualitatively assess the stability of proteinaceous ON, because it is not a common constituent of bacterial peptidoglycans, cannot be degraded by D-amino acid oxidases, and thus, relatively accumulates in soil environments (Amelung, 2003). We also characterized the chemical composition and amino acid enantiomer abundance of mineral-bound ON not extractable into alkaline NaOH–NaF. This ON fraction is considered less degradable because of being less soluble and/or more strongly bonded to minerals.

2. MATERIALS AND METHODS

2.1. Study sites and sampling

Detailed descriptions of the geological, climatic and topographic settings are given elsewhere (Vitousek, 2004; Chorover et al., 2004; Mikutta et al., 2009). Briefly, soils formed in basaltic tephra of ages ranging from 0.3 to 4100 kyr (Table 1). The sites are located at 1130–1500 m above sea level, with a mean annual temperature of 16 °C and a mean annual precipitation of 2500 mm. Soils are classified as Thaptic Udivitrands (site 1, Thurston), Aquic Hydrudands (sites 2–4, Laupahoehoe, Kohala, Pololu), Aquic Hapludands (site 5, Kolekole), and Plinthic Kandiudox (site 6, Kokee) (Chorover et al., 2004). *Metrosideros polymorpha*, an endemic *Myrtaceae*, dominates (>75%) the upper canopy of all sites. Subcanopies are more diverse, including different native tree ferns in the genus *Cibotium*, but the similar chemical composition of organic soil layers (Mikutta et al., 2009; Table 4) suggests a fairly homogeneous composition of OM entering the soils. Vegetation, organic layers, and mineral topsoils (A horizons) and subsoils (B horizons) were sampled in June 2007 and shipped to Germany within four days. In the laboratory, soil samples were pushed through a 2-mm sieve, roots, visible plant and animal remains were removed, and the material was stored field-moist in the dark at 277 K until use.

2.2. Separation and characterization of mineral–organic associations

Mineral–organic associations were separated from the bulk soil by suspending field-moist mineral soil samples in

Table 1
Site age, origin, sampling depth and pH of soil samples, and basic physico-chemical properties of isolated mineral–organic associations from A and B horizons of the Hawaiian long substrate age gradient. Data partly compiled from Chorover et al. (2004) and Mikutta et al. (2009).

	Site age (kyr)	Island	Depth (cm)	Soil pH (H_2O)	SSA (m^2/g)	OC (mg/g)	N (mg/g)	N_{min}[a] (mg/g)	ho ON[b] (%)	OC/ON	After NaOH–NaF extraction			Fe_{dith}[c] (mg/g)	Fe_{ox}[c] (mg/g)	Fe_{ox}/Fe_{dith}	Al_{ox}[c] (mg/g)	Al_{Cu}[d] (mg/g)	Si_{ox}[c] (mg/g)	Clay mineral composition[e]
											OC (mg/g)	N (mg/g)	OC/ON							
A horizons																				
Thurston	0.3	Hawaii	2–9	5.5	2.3	18.7	2.3	0.01	51	8	4.5	0.2	24	5.0	4.3	0.9	2.6	1.5	0.8	P, F, a
Laupahoehoe	20	Hawaii	0–10	4.1	54.4	177.5	9.9	0.03	73	18	70.0	2.5	28	153.6	84.2	0.5	3.3	0.9	0.3	F, A, m, q
Kohala	150	Hawaii	0–7	3.9	28.8	187.6	13.2	0.05	75	14	39.4	2.6	15	46.9	37.4	0.8	18.5	11.1	0.8	A, F, v, hiv, q
Pololu	400	Hawaii	0–10	3.9	19.0	290.4	19.4	0.04	74	15	51.6	2.9	18	43.7	40.0	0.9	7.6	6.1	0.1	A, F, v, hiv, k, q
Kolekole	1400	Molokai	0–-8	4.2	20.2	131.1	9.7	0.01	65	13	40.7	2.2	18	40.1	15.4	0.4	4.2	1.9	0.1	K, Gi, F, he, q
Kokee	4100	Kauai	0–16	4.8	47.6	40.0	2.8	0.01	90	14	16.3	0.5	34	241.3	4.4	0.0	0.4	0.2	0.0	K, Gi, Go, he
B horizons																				
Thurston	0.3	–	15–23	6.1	9.3	23.2	2.5	0.00	72	9	6.2	0.2	25	11.5	10.7	0.9	8.1	1.5	4.1	P, F, a
Laupahoehoe	20	–	45–67	5.3	62.9	113.6	5.6	0.01	50	20	32.0	1.6	21	100.8	77.9	0.8	113.5	7.6	29.5	F, A, m, q
Kohala	150	–	41–60	4.0	55.0	120.6	4.4	0.01	46	27	29.5	1.1	27	15.4	16.9	1.1	137.8	15.9	44.7	A, F, hiv, q
Pololu	400	–	44–64	4.9	65.2	81.3	3.6	0.01	56	23	14.1	0.6	23	124.1	56.6	0.5	50.5	9.2	4.9	A, F, v, hiv, k, q
Kolekole	1400	–	30–49	4.9	64.8	19.9	2.0	0.01	42	10	5.3	0.2	25	53.3	14.4	0.3	14.0	2.4	2.0	K, Gi, f, he, q, m
Kokee	4100	–	50–100	5.2	70.9	12.1	1.6	0.00	22	7	4.5	0.1	48	143.9	2.3	0.0	2.1	0.4	0.1	K, Gi, Go, he, m

[a] Inorganic nitrogen (NO_2^-, NO_3^-, and NH_4^+).
[b] ho ON, hydrophobic ON; XAD-8 fractionation was conducted after extracting mineral–organic associations with 0.1 M NaOH under N_2 atmosphere.
[c] Fe_{dith}, dithionite-extractable Fe; Fe_{ox}, Al_{ox}, Si_{ox}, oxalate-extractable Fe, Al, Si.
[d] Al_{Cu}, $CuCl_2$-extractable Al.
[e] Upper case letters indicate major constituents, lower case letters indicate minor constituents; P, plagioclase; A, short-range-ordered Al gels or aluminosilicates (e.g., allophane), F, ferrihydrite; Q, quartz; V, vermiculite; HIV, hydroxyl-interlayered vermiculite; K, kaolin minerals (kaolinite and/or halloysite); Gi, gibbsite; He, hematite; Go, goethite; M, magnetite..

sodium polytungstate solution of a density of 1.6 g/cm^3 (Mikutta et al., 2009). Subsamples (20 g) of the mineral–organic associations were treated 10 times under N_2 atmosphere with 100 mL 0.1 M NaOH–0.4 M NaF (1:5 wt./vol.) at 295 K, centrifuged (30 min, 4500*g*), carefully decanted, washed with 200 mL deionized H_2O, and freeze-dried. Inorganic N (NO_2^-, NO_3^-, NH_4^+) was extracted into 1 M KCl (1:10 wt./vol.) and determined photometrically (SAN-plus; Skalar Analytical B.V., Breda, The Netherlands). Mineral–organic associations were characterized by selective metal extractions with copper(II) chloride (Juo and Kamprath, 1979), acidic ammonium oxalate (Blakemore et al., 1987), and sodium dithionite–citrate (Blakemore et al., 1987). The specific surface area (SSA) was determined by N_2 adsorption at 77 K (Nova 4200 analyzer, Quantachrome Corp., Boynton Beach, USA). Organic N in the aromatic (hydrophobic) fraction of NaOH-extractable OM was determined by XAD-8 fractionation after acidification (Aiken and Leenheer, 1993). For further details, see Mikutta et al. (2009).

2.3. Radiocarbon dating

Radiocarbon contents of mineral-associated and residual OM (after NaOH–NaF extraction) were measured on graphite targets by accelerator mass spectrometry. $\Delta^{14}C$ values were calculated according to Stuiver and Polach (1977). Prior to graphitization, CO_2 splits were taken to determine the $\delta^{13}C$. $\delta^{13}C$ Values were expressed in ‰ relative to the Pee Dee Belemnite standard. Precision of measured $\delta^{13}C$ values was 0.15‰.

2.4. X-ray photoelectron spectroscopy (XPS) and near edge X-ray absorption fine structure (NEXAFS) analysis

Mineral–organic associations (<200 μm) were analyzed in triplicate by XPS using a PHI 5700 ESCA instrument (Physical Electronics, Chanhassen, MN, USA). Dried samples were pressure-mounted onto indium foil and excited with non-monochromatic Al Kα radiation (E_{exc} = 1486.6 eV; incident angle: 45°; electron beam spot size: 800 μm). The analysis, to a depth of ~3–5 nm, involved a high-resolution scan at the N_{1s} edge using a pass energy of 11.75 eV, a channel width of 0.1 eV/step, and measure time of 100 ms/step (exposition time = 30 min). Vacuum during measurements was $\sim 3 \times 10^{-9}$ mbar. Sample charging during analysis led to peak shifts of ⩽3 eV, which were corrected relative to the principal C_{1s} sub-peak centered at 285 eV. Following Shirley background and Al satellite correction, the chemical composition of ON was estimated by deconvoluting the N_{1s} peak into sub-peaks using additively linked Gaussian–Lorentzian functions by applying the Marquardt algorithm (Unifit for Windows Version 2008; Hesse et al., 2003). Best fitting results were obtained by allowing the Lorentzian part to vary between 0% and 15% and constraining the full-width-at-half maximum (FWHM) between 0 and 2.5. Inorganic N (NO_2^-, NO_3^-, and NH_4^+) was ignored in N_{1s} peak fitting because it comprised <1% of total N (Table 1). The fitted sub-peaks representing different N binding environments were assigned following suggestions by Abe and Watanabe (2004), Abe et al. (2005) and Maie et al. (2006). The sub-peak centered at 399.0 ± 0.2 eV reflects 'aromatic N' including imines, heterocyclic C=N and aromatic amines, that at 400.1 ± 0.1 eV 'peptide N' including pyrrole and secondary and tertiary amines, and imides, and the sub-peak centered at 402.3 ± 0.0 eV is due to primary 'amine N' including protonated amines. The depth profile of ON at the surfaces of mineral–organic associations (taken from A horizons) was analyzed in a representative sample area (~500 μm^2) after sputtering with Ar^+ for 15 min and 30 min. Etching velocity was ~1.4 nm/min for pure SiO_2. Since Ar^+ irradiation can alter the chemical composition of natural OM (Mikutta et al., 2009), we examined NaOH–NaF-extractable OM for Ar^+ treatment-related shifts in N binding environments.

NaOH–NaF-extractable OM was examined by synchrotron-based XP and NEXAFS spectroscopy. The extracted OM was adjusted to pH ~8 with HCl, membrane-filtered (<0.45 μm), dialyzed (molecular-weight cut off of 6000–8000 Dalton) to an electric conductivity of <0.1 mS/dm, and freeze-dried. Thin OM films of ~150–250 nm thickness were spin-coated (Model PWM32; Headway Research, Inc., Garland, TX, USA) on Au wavers at 2000 rpm for 60 s, using suspensions containing 100 g OM/L. Duplicate analyses were performed at the end-station SurICat (beamline PM4) at the synchrotron light source BESSY 2 (Berlin, Germany). Photon energy was referenced to a binding energy of 84 eV for the $Au_{4f7/2}$ core level as measured on freshly prepared polycrystalline Au. The ultrahigh vacuum system consisted of interconnected sample preparation/load lock (base pressure: 1×10^{-8} mbar) and analysis (base pressure: 1×10^{-10} mbar) chambers. Excitation energy for XPS was 620 eV; spectra were collected with a hemispherical electron energy analyzer (SES 100, VG Scienta AB, Uppsala, Sweden) with 100 meV energy resolution (20 eV pass energy). A beam focus of ~1 mm^2 was used to gain representative spectral data for OM and to minimize beam damage. Charging effects can be excluded since no broadening of the photoemission signals was observed. Peak deconvolution of XPS spectra was performed as described above. NEXAFS spectra (photon energy scan between 390 and 420 eV) were collected in energy steps of 100 meV measuring the drain current (I) of the respective specimen relative to the incident drain current measured simultaneously from the refocusing mirror (I_0). Three spectra per sample were averaged, normalized and smoothed (Golay-Savitzky procedure) using WinXAS 3.1 (Ressler, 1998). Transition energy assignment in NEXAFS spectra was done according to Vairavamurthy and Wang (2002) and Leinweber et al. (2007).

2.5. Hydrolyzable amino acid enantiomers

Amino acids in organic soil layers and mineral–organic associations were determined in duplicate after standard HCl hydrolysis (Brodowski et al., 2004). Samples corresponding to 0.5–1 mg N were hydrolyzed in 10 mL of 6 M HCl at 378 K for 12 h. The filtered solution was transferred onto a preconditioned Dowex 50Wx8 resin

(Dow Chemical, Midland, MI, USA) for purification. Interfering metals were removed by rinsing with 0.1 M oxalic acid (pH 1.6–1.7). After elution of amino acids by 2 M NH_4OH, the dried residue was re-dissolved in HCl (pH <2), centrifuged at 5000*g* for 15 min, and transferred into 5-mL reactivials. Samples were freeze-dried and derivatized. The resulting *N*-pentafluoropropionyl-amino acid isopropyl esters were separated and determined using a GCMS-QP 2010 system (Shimadzu Corp., Tokyo, Japan) equipped with a Chirasil-L-Val column (25 m, 0.25 mm inner diameter, 0.12 μm film thickness; Varian, Inc., Palo Alto, CA, USA). Enantiomer concentrations were derived from linear calibration curves obtained with external amino acid enantiomer standards ($r^2 \geqslant 0.999$) by determining the peak area of a specific target ion per substance (Amelung and Brodowski, 2002). Enantioselective separation was not performed for D-serine, losing its Cα proton during mass fragmentation, and D-threonine, where the target ion suffers from unknown proton abstraction (Amelung and Brodowski, 2002). Quantification was done relative to L-norvaline, added to the samples after hydrolysis. D-methionine was used as second internal standard before derivatization. The average recovery of L-norvaline was 90 ± 18% (mean ± standard deviation) for mineral–organic samples and 120 ± 34% of organic soil layers. The total amino acid concentration was calculated as the sum of the D- and L-enantiomers. Hydrolysis transforms glutamine and asparagine, if present, into their carboxylic acids; so we only report concentrations of aspartic acid and glutamic acid. As control, we determined the mass loss during HCl hydrolysis and the fraction of released C and N in a separate experiment, using the same N/HCl ratios as in the original procedure.

2.5.1. Hydrolysis-induced racemization

Hydrolysis-induced racemization in soil samples is hardly predictable but can account for up to 80% of the D-enantiomer (Brodowski et al., 2004). To account for racemization during HCl hydrolysis, hydrolysis was repeated in DCl as described above. Deuterium labels the α-C position during hydrogen abstraction and, hence, changes the T_0 mass fragment by one atomic unit. The hydrolysis-induced racemization (HIR) was estimated according to Brodowski et al. (2004):

$$\mathrm{HIR}\ (\%) = 100\% \times \left[1 - \left(\frac{C_{\mathrm{D,\ DCl}}}{C_{\mathrm{D,\ HCl}}}\right)\left(\frac{C_{\mathrm{L,\ HCl}}}{C_{\mathrm{L,\ DCl}}}\right)\right] \quad (1)$$

where ($C_{\mathrm{D,HCl}}$), ($C_{\mathrm{D,DCl}}$), and ($C_{\mathrm{L,HCl}}$), ($C_{\mathrm{L,DCl}}$) correspond to the D- and L-amino acid enantiomers in the HCl and DCl hydrolysate. If the D-enantiomer was <1 μg/g, D/L ratios were not corrected for HIR. Based on the HIR, the apparent enantiomer ratio was calculated by subtracting the proportion of the D-enantiomer formed during hydrolysis from the measured D-enantiomer concentration and adding it to the respective L-enantiomer concentration. The analytical error of L-enantiomer duplicates was <10% for most amino acids (8.3 ± 4.4; mean ± standard deviation); for the D-enantiomers the average error was 26 ± 16% due to their small abundances. The HIR was smallest for alanine, ranging from 0% to 21% (7 ± 7%), and for lysine, ranging from 0% to 60% (22 ± 22%). For other amino acids, it frequently reached 100% (Table EA 1). Hence, the apparent D/L ratios of amino acids other than alanine and lysine should be considered with caution.

2.6. Hydrolyzable amino sugars

Amino sugars (glucosamine, mannosamine, galactosamine, muramic acid) in organic soil layers and mineral–organic samples were determined in duplicate according to Zhang and Amelung (1996). Briefly, after adding 100 μg myo-inositol as first internal standard to samples (corresponding to 0.5–1 mg N), they were hydrolyzed in 6 M HCl at 378 K for 8 h. Hydrolysates were filtered and impurities precipitated by neutralization with 0.4 M KOH. 3-*O*-Methylglucose was added as second internal standard. Aldonitril acetate amino sugar derivates were analyzed using a gas chromatograph with flame ionization detector (GC-2010, Shimadzu Corp., Tokyo, Japan) equipped with a SPB-5 fused silica column (30 m, 0.25 inner diameter, 0.25-μm film; Supelco, Bellefonte, PA). Quantification was done from linear or quadratic calibration curves obtained with external amino sugar standards ($r^2 \geqslant 0.999$) relative to myo-inositol. The average recovery of myo-inositol was 70 ± 2% for mineral–organic samples and 86 ± 18% for organic soil layers.

Muramic acid (MurA) is unique to peptidoglycan of bacterial cell walls (Kögel-Knabner, 2002) but may, in traces, also derive from actinomycetes (Glaser et al., 2003). Glucosamine (GlcN) primarily derives from chitin (*N*-acetylglucosamine) of fungi and arthropodes, hence, the GlcN/MurA ratio informs on the contribution of fungal and bacterial remains (Guggenberger et al., 1999).

2.7. Estimation of non-hydrolyzable peptide nitrogen

Proportions of not hydrolyzed peptide N (Pep-N_{nhydr}) were estimated using the amino acid (AA-N) and amino sugar (AS-N) data and the XPS peptide N sub-peak at 400.1 eV:

$$\mathrm{Pep-N_{nhydr}}(\%) = \frac{(\mathrm{AA-N + AS-N})\ (\mu g/g) \times 100\%}{[\mathrm{Pep-N_{XPS}}(\%) \times \text{total ON}(\mu g/g)/100\%]} \quad (2)$$

This calculations assumes polymeric compounds such as proteins, chitin, and peptidoglycan to be the dominant sources of hydrolyzable N. Since (i) XPS covers only N species at particle surfaces and (ii) other N species might contribute to XPS signals in the peptide region, this calculation gives a tentative estimate of not hydrolyzed peptide N.

2.8. Definitions and statistics

Pearson correlation coefficients between test variables were calculated based on *z*-transformed variables using Statistica 5.1 (StatSoft Inc., Tulsa, USA). Deviations from mean values are reported as standard deviation.

3. RESULTS

3.1. Organic N contents and OC/ON ratios of mineral–organic associations

Organic N in mineral–organic associations ranged from 2 to 19 mg/g (Table 1) and accounted for 88 ± 4% of the total N in the respective soil horizons (Mikutta et al., 2009). Inorganic N (NO_2^-, NO_3^-, and NH_4^+) contributed to <1% to total soil N. Mineral-associated ON in A horizons increased from the youngest (0.3 kyr) to the 20–400-kyr sites and finally decreased at the oldest sites (1400 and 4100 kyr). Despite the large ON concentrations, OC/ON ratios were widest at the intermediate-aged sites, particularly in the subsoil. The OC/ON ratio significantly correlated with oxalate-extractable Al and Si, and $CuCl_2$-extractable Al ($r = 0.80$, 0.73, 0.77; $p < 0.01$; $n = 12$). Mineral-associated ON was more prone to extraction into NaOH–NaF (A horizons: 82 ± 6%; B horizons: 84 ± 9%) than OC (A horizons: 71 ± 10%; B horizons: 73 ± 6%). In consequence, the OC/ON ratios of solid-phase residues increased (Table 1), indicating OM strongly bound to minerals to be depleted in ON. Fractionation with XAD-8 showed that the majority of the alkaline-extractable mineral-associated ON was with hydrophobic OM (71 ± 13%) in topsoils, while it was only 48 ± 17% in subsoils (Table 1).

3.2. ^{14}C ages and $\delta^{13}C$ values

Mineral-bound OM in most A horizons comprised recently fixed C ($\Delta^{14}C = 2$–126‰) but had negative $\Delta^{14}C$ at two sites (Laupahoehoe, 20 kyr and Kokee, 4100 kyr), revealing a larger fraction of aged OM (Table 2). The same two A horizons also contained the largest mass of dithionite-extractable Fe (Table 1). Nearly all subsoil mineral-associated OM had negative $\Delta^{14}C$ values ($\Delta^{14}C = 24$ to −768‰), indicating a predominance of older C. The $\delta^{13}C$ values of mineral-associated OM showed little across-site variation (A horizons: −26.3 ± 0.3‰; B horizons: −25.5 ± 0.5‰). The enrichment in ^{13}C as compared with the respective topsoils (mean difference = 0.8‰; $n = 12$) suggests somewhat more hydrophilic OM in subsoils. Extracting with NaOH–NaF removed OM with less negative $\Delta^{14}C$ values from topsoil mineral–organic associations; for subsoils, the response was inconsistent, with four of the NaOH–NaF residues having more positive $\Delta^{14}C$ values (Table 2).

3.3. Nitrogen XPS of organic matter in mineral–organic associations

Fig. 1A depicts the deconvoluted N_{1s} XP spectrum of the 0.3 kyr topsoil mineral–organic associations; deconvolution results of all samples are summarized in Table 3.

Table 2
Radiocarbon data and ^{13}C isotopic ratios of mineral–organic associations from A- and B horizons of the Hawaiian long substrate age gradient before and after extraction with 0.1 M NaOH–0.4 M NaF. Values in parenthesis refer to the standard deviation of the mean.

Site age (kyr)	$\delta^{13}C$ (‰)	Fraction modern		$\Delta^{14}C$ (‰)	
A horizons					
0.3	−26.3	1.1339	(0.0021)	126.0	(2.1)
20	−26.9	0.9515	(0.0016)	−55.1	(1.6)
150	−26.1	1.0906	(0.0019)	82.9	(1.9)
400	−26.4	1.0089	(0.0017)	1.8	(1.7)
1400	−25.9	1.0668	(0.0018)	59.4	(1.8)
4100	−26.2	0.8753	(0.0016)	−130.9	(1.6)
B horizons					
0.3	−25.4	1.0307	(0.0018)	23.5	(1.8)
20	−25.5	0.4647	(0.0009)	−538.6	(0.9)
150	−26.0	0.3845	(0.0009)	−618.2	(0.9)
400	−25.7	0.4379	(0.0009)	−565.2	(0.9)
1400	−25.7	0.5237	(0.0013)	−479.9	(1.3)
4100	−24.5	0.2336	(0.0007)	−768.1	(0.7)
A horizons after NaOH–NaF extraction					
0.3	−23.0	1.0114	(0.0019)	4.3	(1.9)
20	−26.8	0.9071	(0.0016)	−99.3	(1.6)
150	−25.6	1.0459	(0.0020)	38.6	(2.0)
400	−26.6	0.9823	(0.0017)	−24.5	(1.7)
1400	−25.7	1.0366	(0.0019)	29.3	(1.9)
4100	−25.5	0.7857	(0.0015)	−219.8	(1.5)
B horizons after NaOH–NaF extraction					
0.3	−24.5	1.0197	(0.0019)	12.5	(1.9)
20	−24.4	0.4880	(0.0010)	−515.4	(1.0)
150	−24.8	0.4482	(0.0009)	−554.9	(0.9)
400	−24.8	0.4338	(0.0012)	−569.3	(1.2)
1400	−23.7	0.7323	(0.0014)	−272.8	(1.4)
4100	−22.9	0.4281	(0.0010)	−574.9	(1.0)

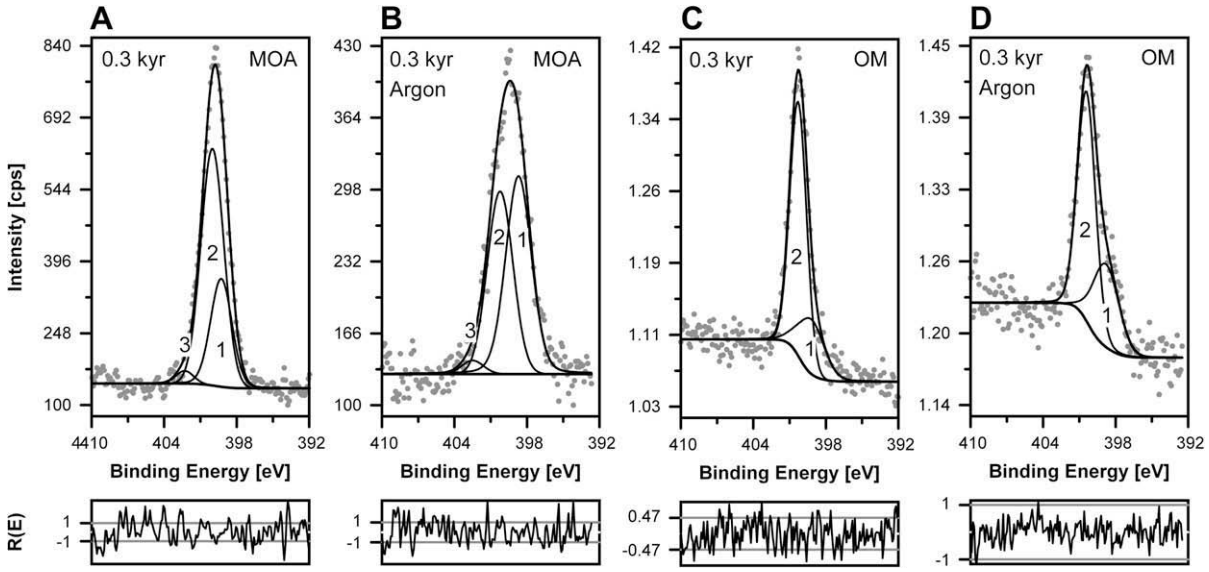

Fig. 1. Representative N_{1s} XP spectra of the mineral–organic association from the A horizon of the 0.3-kyr site (A) before and (B) after Ar^+ sputtering. Effect of Ar^+ gassing on N functional groups in pure OM extracted from the 0.3-kyr mineral–organic association: (C) untreated and (D) Ar^+-treated. Binding energies denote: 1 = aromatic N (399.0 ± 0.2 eV), 2 = peptide N (400.1 ± 0.1 eV), and 3 = primary amine N (402.3 ± 0.0 eV). Note, that the intensity in C and D is given kcps instead of cps. Excitation energy was 1486.6 eV.

The results reveal the composition of outermost layers (*ca.* 3–5 nm) of mineral-bound OM. Aromatic, peptide and primary amine N accounted for 18–33%, 64–78%, and 3–8% of mineral-associated ON in topsoils and for 21–34%, 59–75%, and 2–7% in subsoils. Amide N was always the predominant N form (Table 3). Roughly, one quarter of total ON was in aromatic compounds and ≪10% was in primary amines. On a mass basis, no relationship of N species with mineral phase variables was found for topsoils. In subsoils, aromatic and peptide N correlated positively with oxalate-extractable Fe + Al + Si ($r = 0.93$ and 0.97; $p < 0.05$) whereas primary amine N correlated with oxalate-extractable Fe ($r = 0.91$; $p < 0.05$). Abrasion of topsoil particles by Ar^+ caused a roughly simultaneous decline in C and N with abrasion depth. The decline in C during 15 and 30 min Ar^+ irradiation strongly correlated with that in N ($r = 0.95$; $p < 0.01$, and 0.78; $p = 0.07$). The Ar^+ sputtering revealed a pronounced increase in C–C/C–H bonds of aromatic moieties (284.4 eV), which was not an artifact caused by the Ar^+ bombardment (Mikutta et al., 2009). In contrast, the increase in aromatic N and the decline in peptide N can be attributed to the differing stability of N structures

Table 3
Organic N binding environments in mineral–organic associations of the Hawaiian long substrate age gradient as revealed by XPS (in atom%). Values in parenthesis refer to the standard deviation of the mean of triplicate measurements. Values following the slash (/) refer to the average full-width-at-half maximum (FWHM) values of the deconvoluted peaks ($n = 3$).

	Site age (kyr)	Aromatic N 399.0 ± 0.2 eV[a]	Peptide N 400.1 ± 0.1 eV[a]	Primary amine N 402.3 ± 0.0 eV[a]
A horizons				
Thurston	0.3	32.5 (2.7)/2.3	63.5 (3.9)/2.1	3.9 (1.3)/1.6
Laupahoehoe	20	18.3 (1.8)/2.4	77.8 (1.9)/2.2	3.9 (0.1)/1.5
Kohala	150	18.5 (1.6)/2.2	77.0 (1.6)/2.3	4.5 (0.2)/1.3
Pololu	400	30.7 (0.4)/2.3	64.8 (1.3)/2.1	4.5 (1.8)/1.3
Kolekole	1400	19.9 (0.1)/2.0	71.7 (1.0)/2.2	8.4 (0.9)/1.7
Kokee	4100	30.8 (1.5)/2.1	66.1 (2.6)/2.1	3.1 (2.5)/1.3
Mean (SD)		25.1 (6.9)	70.1 (6.3)	4.7 (1.9)
B horizons				
Thurston	0.3	33.2 (2.1)/2.5	64.8 (2.3)/2.2	2.0 (1.0)/1.5
Laupahoehoe	20	21.1 (2.1)/2.5	74.6 (2.3)/2.3	4.3 (0.8)/1.1
Kohala	150	27.2 (0.4)/2.3	70.8 (0.9)/2.3	2.1 (1.2)/0.8
Pololu	400	28.0 (1.4)/2.3	64.6 (0.8)/2.2	7.4 (1.5)/1.4
Kolekole	1400	34.3 (2.7)/2.3	58.9 (2.2)/2.3	6.9 (4.4)/1.7
Kokee	4100	29.6 (3.6)/2.2	66.3 (5.5)/2.5	4.1 (3.9)/1.5
Mean (SD)		28.9 (4.1)	66.7 (5.5)	4.5 (2.3)

[a] Average binding energy ± standard deviation of all fitted samples.

under Ar^+ irradiation (Fig. 1A and B and Table EA 2). While aromatic structures in natural OM appear less stable (Mikutta et al., 2009), Ar^+ irradiation of OM extracted from 0.3-kyr topsoil mineral–organic associations for 5 min caused a selective loss of peptide N (by 7.4%) in favor of aromatic N (Fig. 1C and D). This suggests amino groups to be even more sensitive to Ar^+ bombardment than aromatic structures, thus, unambiguous inferences about the location of aromatic versus peptide N at particle surfaces are not possible.

3.4. Nitrogen XPS and NEXAFS of extracted organic matter

Since XPS analysis of powder samples is limited to external particle surfaces, we examined extractable OM by synchrotron XPS and NEXAFS, which provides the composition of most of the sorbed ON. The XP spectra of OM films showed a smaller signal-to-noise ratio than those of conventional XPS analyses (Fig. 2), which did not permit an unequivocal assignment to N binding environments, particularly when the abundance of sub-components (primary amines) was small. The shape of the N_{1s} peaks, however, suggests the predominance of peptide N. Sub-peak deconvolution revealed even more peptide N in extracted OM (A horizons: $\sim 88 \pm 4\%$, B horizons: $\sim 96 \pm 2\%$; $n = 8$) than in powder samples. No reliable XP and NEXAFS spectra were obtained for OM from the 0.3 and 150 kyr sites, likely because of insufficient electron yields. In accordance with the peptide-dominated nature of ON, the N K-edge NEXAFS spectra showed little spectral and site variability (Fig. 3). The prominent peak located near the N ionization threshold at around 402.5 eV represents 1s → π* transitions of N coupled to C═O structures in amides (Vairamurthy and Wang, 2002). Pyrrole and imidazole N may also contribute to this signal while imidazole derivatives generate additional peaks or shoulders at <400 eV (Leinweber et al., 2007). The NEXAFS spectra showed some pre-edge features at around 399.8 eV, likely due to pyridine and other minor compounds such as imidazoles or pyrimidines. In cases where the spectral resolution was poor (e.g., OM from subsoil mineral–organic associations of the 20 kyr site; Fig. 3), the pre-edge resonances could not be discerned from background signals or beam damage. Leinweber et al. (2007) found resonances between 399 and 400 eV when exposing methionine and arginine to X-ray radiation (10^{11} photoelectrons/s at 0.8 mm × 0.2 mm beam spot size). Although beam damage is less likely for our setup (3.2×10^9 photoelectrons/s at 1 × 1 mm beam spot size), we did not deconvolute the NEXAFS spectra because of the potential uncertainties.

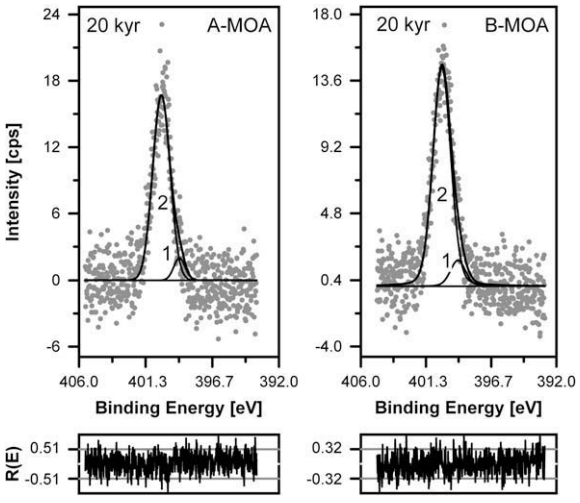

Fig. 2. Two representative synchrotron-based N_{1s} XP spectra obtained for OM that derived from mineral–organic associations of the A horizon (A-MOA) and B horizon (B-MOA) of the 20-kyr site. Binding energies denote: 1 = aromatic N (399.0 ± 0.2 eV) and 2 = peptide N (401.0 ± 0.1 eV). No peak could be fitted in the 402.3 ± 0.0 eV region representing primary amine N. Incident photon energy was 620 eV.

3.5. Amino acids and amino sugars in mineral–organic associations

3.5.1. Concentrations of hydrolyzable amino acids and amino sugars

3.5.1.1. Amino acids. Concentrations of hydrolyzable amino acids across the soil gradient were smaller than or comparable to those of plant source materials (leaves) and organic soil layers (L and O horizons) (Fig. 4A and Table 4). Acid hydrolysis reduced sample weights by 21–84% because of substantial dissolution of mineral phases. Mineral-associated N was released to larger extent (A horizons: 89 ± 3%; B horizons: 95 ± 3%) than OC (A horizons: 55 ± 7%; B horizons: 89 ± 6%). Amino acid concentrations in topsoil mineral–organic associations were smallest at the youngest and oldest site (0.3 and 4100 kyr) and largest at the intermediate-aged sites (150 kyr and 400 kyr) rich in poorly crystalline minerals and metal(hydroxide)–organic precipitates (Fig. 4A). Hydrolyzable amino acids correlated well with mineral-associated OC ($r = 0.90$; $p < 0.001$) and ON (0.96: $p < 0.001$) but less with mineral variables. Topsoil amino acids showed an insignificant relationship with oxalate-extractable Fe + Al ($r = 0.79$; $p = 0.06$) and those in subsoils with oxalate-extractable Fe ($r = 0.77$: $p = 0.07$). The portion of N identified as amino acid N in topsoil mineral–organic associations ranged from 11% to 26% (18.8 ± 5.8%), with the largest contribution at the 20-kyr site (Table 4); the portion of C with hydrolyzable amino acids ranged between 3% and 7% (4.9 ± 1.6%). Yields for subsoil mineral–organic associations were smaller, with <14% of the N (6.3 ± 5.3%) and <5% of the C (1.6 ± 1.8%) in hydrolyzable amino acids. Amino acid concentrations peaked at the 400-kyr site for topsoils. For subsoils the maximum occurred at the 20 kyr site, and then concentrations declined gradually with substrate age (Fig. 4A).

3.5.1.2. Amino sugars. Concentrations of hydrolyzable amino sugars in litter layers were variable across sites but significantly increased in O layers to a roughly constant level, which exceeded that of most mineral–organic associations (Fig. 4B). Hydrolyzable amino sugars were most

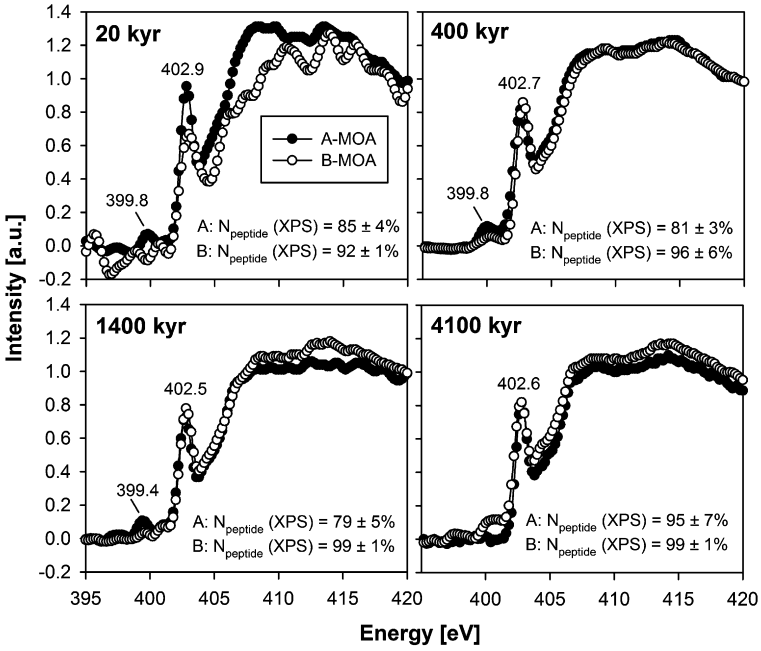

Fig. 3. Nitrogen K-edge NEXAFS spectra of films prepared of OM extracted by 0.1 M NaOH–0.4 M NaF from mineral–organic associations of A horizons (A-MOA) and B horizons (B-MOA) of the Hawaiian long substrate age gradient. No reliable spectra were obtained for the 0.3- and 150-kyr site. For the OM films, we additionally provide the estimated spectral contribution of peptide N as analyzed by synchrotron-based XPS.

concentrated in topsoil mineral–organic associations during the intermediate weathering stage until 400-kyr, then dropped towards the oldest site. The portion of N with hydrolyzable amino sugars varied between 4% and 9% ($6.2 \pm 2.0\%$); those of C ranged between 3% and 8% ($5.8 \pm 2.2\%$). In the subsoil, yields were up to one order of magnitude smaller than in topsoils and followed a pattern similar that of the amino acids (Fig. 4A and B). Less than 4% of N ($3.3 \pm 0.7\%$) and <5% of C ($3.1 \pm 1.4\%$) was in hydrolyzable amino sugars. Total hydrolyzable amino sugars in topsoils were weakly related to mineral phase variables but strongly with mineral-associated OC ($r = 0.89$; $p < 0.001$) and ON ($r = 0.96$; $p < 0.001$). In subsoils, amino sugars related to OC and ON ($r = 0.84$ and 0.97), but also to oxalate-extractable Fe + Al ($r = 0.92$; $p < 0.01$).

3.5.2. Non-hydrolyzable peptide nitrogen

We estimate that *ca.* 58–78% of mineral-associated peptide N in topsoils was not hydrolyzed (Fig. 4C). Irrespective of the exact amount, a large portion of mineral-associated peptide N seems to be in hydrolysis-resistant structures, thus escaping analytical assessment. The proportion of non-hydrolyzable peptide N in topsoils was smallest at 20–400 kyr; for subsoils, it steadily increased towards the older sites (Fig. 4C). Significantly more peptide N resisted hydrolysis in subsoil than in topsoil mineral–organic associations (Fig. 4C). The fraction of non-hydrolyzable peptide N thus increased with mean horizon depth ($r = 0.88$; $p < 0.001$) and with decreasing $\Delta^{14}C$ ($r = -0.90$; $p < 0.001$), i.e., with ^{14}C age of mineral-associated OM (Fig. 6A). Non-hydrolyzability of peptide N was not significantly related to most mineral variables, but depended on the crystallinity of Fe minerals (Fig. 7A). In addition, more hydrolysis-resistant peptide N was present at older sites where the volumetric OM–mineral ratios were smaller (Fig. 7B).

3.5.3. Composition of N compound classes and their contribution to mineral-associated organic matter

3.5.3.1. Amino acids. The composition of hydrolyzable amino acids in topsoil mineral–organic associations varied only slightly across sites (Table 4), with glycine and alanine being most abundant, followed by aspartic acid > glutamic acid > valine > serine > others. For subsoils, the order was: alanine = glycine > glutamic acid = aspartic acid > lysine > valine > others. The contribution of individual amino acids across the gradient varied by <2 mol% (standard deviation) for topsoils. A larger variability was observed for subsoils, especially for the acidic amino acids (Asp, Glu) and the basic amino acid lysine (Table 4). Neutral amino acids generally dominated in all samples (72 ± 5 mol%; Fig. 4D). In topsoil mineral–organic associations, lysine was least abundant at 20–400 kyr while acidic amino acids were least at the oldest site. Acidic amino acids in subsoil mineral–organic associations were most prominent at 20–400 kyr, which went along with the minimum contributions of lysine and neutral amino acids (Fig. 4D). These compounds were most abundant at the youngest and the oldest site. The molar ratio of acidic/basic amino acids [(Asp + Glu)/Lys] as well as the ratio of acidic/neutral amino acids correlated strongly with $CuCl_2$-extractable Al ($r = 0.71$ and 0.79; $p < 0.01$; $n = 12$) and oxalate-extractable Fe + Al + Si (Fig. 8). Carbon-normalized amino acid concentrations in

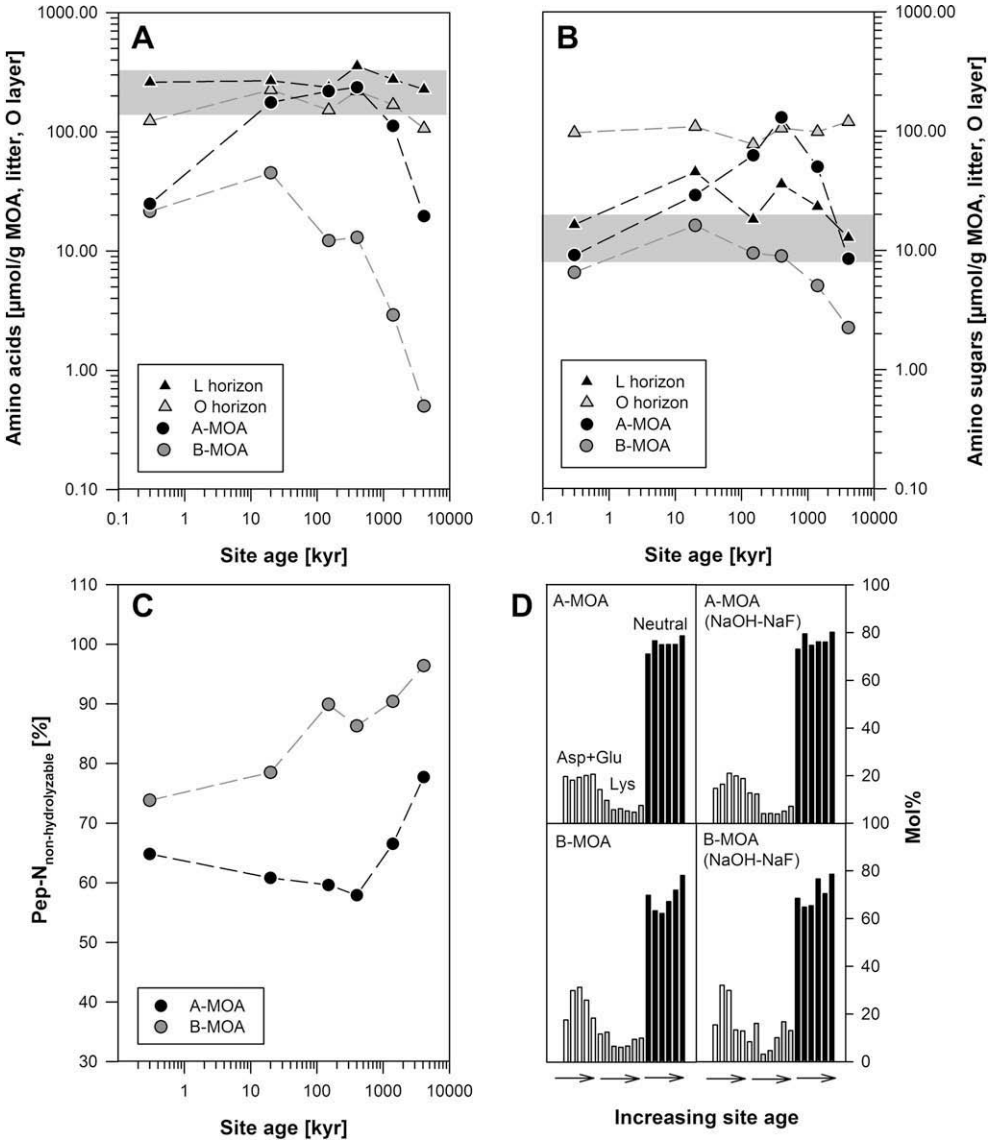

Fig. 4. (A) and (B) Concentration of hydrolyzable amino acids and amino sugars in organic soil horizons (L and O) and mineral–organic associations from A horizons (A-MOA) and B horizons (B-MOA) across the Hawaiian long substrate age gradient. Gray bands indicate the range of amino acid and amino sugar concentrations in living leaves of collected plant sources. (C) Estimated contribution of peptide N not hydrolyzed in HCl as calculated with Eq. (2). (D) Time-dependent mol%-contribution of acidic (Asp + Glu), basic (lysine), and neutral amino acids (Ala, Val, Thr, Gly, Ile, Pro, Leu, Ser, Phe, L-Met, Tyr) to the hydrolyzable amino acid fraction in mineral–organic associations and in mineral–organic associations following extraction with 0.1 M NaOH–0.4 M NaF.

topsoil mineral–organic associations were maximal at the 0.3-kyr site and steadily declined towards the oldest site (Fig. 9). Except for the youngest site, less amino acids were found in subsoil mineral–organic associations, also declining steadily towards the older sites (not shown).

3.5.3.2. Amino sugars. Hydrolyzable amino sugars were dominated by glucosamine, followed by galactosamine, muramic acid, and mannosamine (Table 5). Across the sites, particularly in topsoils, the mass ratio of glucosamine to muramic acid (GlcN/MurA) was variable but tended to increase at older sites (Fig. 5A). No relationship with pH and mineral phase variables was found. With soil depth, the contribution of muramic acid increased at the expense of glucosamine (Table 5). Across all samples, GlcN/MurA was correlated negatively with the mean horizon depth ($r = -0.76$; $p < 0.01$). The amino sugar/amino acid ratio of topsoil mineral–organic associations varied little (0.3–0.9; Fig. 5B). For subsoils, it continuously increased towards the older sites (0.4–7.4). Like for amino acids, OC-normalized amino sugar yields were largest in topsoils of the 0.3-kyr site. After a minimum at 20 kyr, mineral-associated amino sugars increased towards the 400 kyr site, then decreased again at the oldest sites (Fig. 9).

3.5.4. Amino acid D- and L-enantiomers

D-enantiomers of alanine, aspartic acid, glutamic acid, and lysine could be detected, for other amino acids, the

Table 4
Concentration and composition of hydrolyzable amino acids (AA) in organic soil layers, mineral–organic associations, and mineral–organic associations after NaOH–NaF extraction along the Hawaiian long substrate age gradient. *Abbreviations:* Ala, alanine; Val, valine; Thr, threonine; Gly, glycine; Ile, isoleucine; Pro, proline; Leu, leucine; L-Meth, L-methionine; Phe, phenylalanine; Asp, aspartic acid + asparagine; Glu, glutamic acid + glutamine; Tyr, tyrosine; Lys, lysine; AA-C, C in hydrolyzable amino acids; AA-N, N in hydrolyzable amino acids.

Site age (kyr)	Ala	Val	Thr	Gly	Ile	Pro	Leu	Ser	L-Met	Phe	Asp	Glu	Tyr	Lys	Total	AA-C	AA-N
Organic soil layers																	
L horizons (μmol/g)																(%)	(%)
0.3	13.9	7.6	8.6	12.4	5.1	12.0	11.3	9.4	1.4	6.6	11.8	13.2	2.6	7.2	123.2	1.3	70.8
20	24.4	14.3	15.0	21.6	9.7	22.2	20.6	17.2	2.0	12.5	20.8	23.3	6.1	14.9	224.8	2.4	71.4
150	19.3	10.0	10.4	16.1	6.4	14.1	14.2	10.9	1.5	8.1	13.3	15.2	3.3	9.2	152.1	1.6	72.3
400	26.5	13.4	14.1	27.9	9.0	21.1	20.7	17.4	1.9	10.7	18.8	21.0	3.9	13.8	220.2	2.3	71.4
1400	21.3	10.9	11.9	17.1	6.8	15.4	15.3	12.5	1.5	8.8	14.8	17.3	3.9	11.2	168.6	1.8	70.7
4100	14.8	6.2	7.2	13.5	3.5	9.8	9.6	8.0	1.0	5.3	9.5	11.1	2.1	4.9	106.4	1.2	72.9
O horizons (μmol/g)																	
0.3	28.4	13.7	18.5	39.6	8.3	26.3	19.0	23.4	1.0	10.0	26.8	26.3	4.6	14.3	260.1	2.9	76.7
20	33.2	14.3	16.7	41.2	8.3	22.8	20.3	22.1	0.7	11.1	30.0	26.4	5.2	15.0	267.4	3.1	80.9
150	28.7	14.1	16.6	36.4	8.1	21.5	16.5	21.1	1.0	8.8	24.5	22.5	3.7	11.9	235.6	3.3	79.3
400	44.1	20.1	25.0	56.9	10.9	33.2	24.2	32.7	1.5	12.9	36.8	33.5	5.4	18.7	356.0	3.5	77.3
1400	31.4	18.8	21.9	38.4	10.5	22.2	20.4	22.9	1.5	10.9	28.3	24.6	4.5	18.5	274.7	3.5	76.0
4100	28.6	12.5	14.8	36.7	6.8	19.8	15.4	20.9	0.9	8.6	23.9	20.7	3.9	12.8	226.1	2.6	80.0
L horizons (mol%)																	
0.3	11.3	6.2	7.0	10.1	4.2	9.7	9.2	7.7	1.1	5.3	9.6	10.7	2.1	5.9	100.0	—	—
20	10.9	6.4	6.7	9.6	4.3	9.9	9.2	7.6	0.9	5.6	9.3	10.4	2.7	6.6	100.0	—	—
150	12.7	6.6	6.8	10.6	4.2	9.3	9.3	7.2	1.0	5.3	8.8	10.0	2.2	6.1	100.0	—	—
400	12.0	6.1	6.4	12.7	4.1	9.6	9.4	7.9	0.9	4.8	8.6	9.5	1.8	6.3	100.0	—	—
1400	12.7	6.5	7.0	10.1	4.0	9.1	9.0	7.4	0.9	5.2	8.8	10.3	2.3	6.6	100.0	—	—
4100	13.9	5.8	6.7	12.6	3.3	9.2	9.0	7.5	0.9	5.0	8.9	10.5	1.9	4.6	100.0	—	—
O horizons (mol%)																	
0.3	10.9	5.3	7.1	15.2	3.2	10.1	7.3	9.0	0.4	3.9	10.3	10.1	1.8	5.5	100.0	—	—
20	12.4	5.4	6.2	15.4	3.1	8.5	7.6	8.3	0.3	4.2	11.2	9.9	2.0	5.6	100.0	—	—
150	12.2	6.0	7.0	15.5	3.5	9.1	7.0	8.9	0.4	3.7	10.4	9.5	1.6	5.1	100.0	—	—
400	12.4	5.6	7.0	16.0	3.1	9.3	6.8	9.2	0.4	3.6	10.3	9.4	1.5	5.3	100.0	—	—
1400	11.4	6.8	8.0	14.0	3.8	8.1	7.4	8.3	0.5	4.0	10.3	8.9	1.6	6.7	100.0	—	—
4100	12.6	5.5	6.5	16.2	3.0	8.8	6.8	9.2	0.4	3.8	10.6	9.1	1.7	5.6	100.0	—	—
Mineral–organic associations																	
A horizons (μmol/g MOA)																	
0.3	3.0	2.2	1.5	3.6	1.2	1.8	1.7	1.3	0.1	0.9	2.4	2.4	0.3	2.4	24.8	7.1	16.8
20	24.5	15.9	12.9	27.3	8.2	11.1	12.3	11.6	1.0	7.3	17.8	14.0	2.5	9.9	176.1	5.2	26.4
150	31.2	18.4	15.3	37.0	9.2	12.5	14.0	14.4	0.6	7.7	23.6	18.4	3.6	13.0	218.8	6.0	24.5
400	35.5	16.5	19.1	37.9	8.2	13.2	14.3	19.7	0.5	8.2	25.8	21.4	3.1	11.9	235.4	4.1	17.9
1400	17.0	6.2	8.0	20.0	2.9	6.8	6.8	9.8	0.5	3.8	12.5	10.4	2.0	5.1	111.9	4.2	16.8
4100	3.1	1.5	0.7	3.1	0.8	1.5	1.7	1.3	0.1	1.0	1.6	1.2	0.5	1.5	19.6	2.6	10.5

B horizons (μmol/g MOA)																
0.3	2.8	1.9	1.0	3.3	1.0	1.7	1.6	0.7	0.1	0.8	1.7	2.1	0.2	2.7	21.5	5.0	13.4
20	7.0	3.8	2.4	6.3	1.6	2.2	2.1	1.8	0.2	1.0	7.4	6.1	0.2	3.0	45.1	2.0	12.0
150	1.6	0.7	0.7	2.0	0.3	0.6	0.7	0.6	0.0	0.4	2.3	1.6	0.2	0.8	12.2	0.5	4.1
400	2.0	0.8	0.8	2.2	0.4	0.6	0.6	0.8	0.1	0.3	1.7	1.7	0.1	0.9	13.0	0.8	5.4
1400	0.4	0.2	0.1	0.4	0.1	0.3	0.2	0.1	0.0	0.1	0.2	0.4	0.0	0.3	2.9	0.8	2.2
4100	0.1	0.0	0.0	0.1	0.0	0.0	0.0	0.0	0.0	0.0	0.0	0.0	0.0	0.1	0.5	0.2	0.5
A horizons (mol%)																
0.3	12.3	8.7	5.9	14.6	4.8	7.1	7.0	5.2	0.6	3.5	9.8	9.7	1.3	9.5	100.0	—	—
20	13.9	9.0	7.3	15.5	4.7	6.3	7.0	6.6	0.6	4.2	10.1	8.0	1.4	5.6	100.0	—	—
150	14.3	8.4	7.0	16.9	4.2	5.7	6.4	6.6	0.3	3.5	10.8	8.4	1.6	6.0	100.0	—	—
400	15.1	7.0	8.1	16.1	3.5	5.6	6.1	8.4	0.2	3.5	11.0	9.1	1.3	5.1	100.0	—	—
1400	15.2	5.5	7.2	17.9	2.6	6.0	6.1	8.8	0.4	3.4	11.2	9.3	1.8	4.6	100.0	—	—
4100	15.7	7.8	3.6	16.0	4.1	7.6	8.8	6.9	0.5	5.2	7.9	6.1	2.3	7.4	100.0	—	—
B horizons (mol%)																
0.3	12.9	8.7	4.5	15.2	4.8	7.9	7.4	3.3	0.5	3.6	8.0	9.6	1.1	12.5	100.0	—	—
20	15.5	8.4	5.3	13.9	3.7	4.8	4.6	3.9	0.4	2.3	16.5	13.5	0.5	6.6	100.0	—	—
150	12.9	5.5	5.6	16.1	2.6	5.1	5.4	4.5	0.0	3.2	18.4	13.0	1.4	6.2	100.0	—	—
400	15.2	6.4	6.4	17.2	3.0	4.6	4.8	5.8	0.4	2.6	13.2	12.8	0.9	6.7	100.0	—	—
1400	15.0	7.3	5.1	13.2	3.9	9.3	8.3	4.0	0.0	4.5	6.4	12.0	1.5	9.5	100.0	—	—
4100	20.2	7.8	5.1	15.2	3.0	8.3	8.5	4.5	0.0	4.5	3.4	8.3	1.2	10.1	100.0	—	—
Mineral–organic associations after NaOH–NaF extraction																
A horizons (μmol/g MOA)																
0.3	0.2	0.1	0.0	0.2	0.1	0.1	0.2	0.0	0.0	0.1	0.1	0.1	0.0	0.2	1.5	1.8	12.1
20	6.1	2.6	2.1	6.4	1.8	3.0	3.7	2.3	0.2	2.3	3.4	3.1	0.9	1.6	39.3	2.0	15.2
150	7.7	2.9	2.7	8.3	1.7	3.5	4.1	3.1	0.3	2.4	5.1	5.6	1.5	2.2	50.9	3.7	15.7
400	12.4	2.5	4.4	11.5	2.7	5.5	6.3	5.0	0.5	3.5	6.9	7.9	2.2	2.9	74.2	3.2	15.6
1400	3.3	1.4	1.3	4.0	1.0	2.1	2.4	1.6	0.2	1.4	2.5	2.4	0.9	1.3	25.7	2.6	12.8
4100	0.8	0.4	0.2	0.7	0.3	0.5	0.7	0.2	0.0	0.4	0.3	0.4	0.1	0.4	5.3	1.7	14.8
B horizons (μmol/g MOA)																
0.3	0.3	0.1	0.0	0.2	0.1	0.2	0.2	0.0	0.0	0.1	0.1	0.2	0.0	0.3	1.8	1.6	11.2
20	2.3	1.0	0.6	2.2	0.5	0.8	1.0	0.6	0.1	0.6	2.9	1.9	0.1	0.5	14.9	1.8	10.6
150	1.1	0.5	0.3	1.0	0.3	0.5	0.7	0.2	0.1	0.5	1.5	1.0	0.1	0.4	8.3	1.1	8.3
400	0.4	0.2	0.1	0.4	0.2	0.2	0.3	0.1	0.0	0.2	0.2	0.2	0.1	0.3	2.7	0.7	4.6
1400	0.1	0.1	0.0	0.0	0.1	0.1	0.1	0.0	0.0	0.1	0.0	0.1	0.0	0.1	0.9	0.9	6.0
4100	0.0	0.0	0.0	0.0	0.0	0.0	0.0	0.0	0.0	0.0	0.0	0.0	0.0	0.0	0.2	0.3	3.6
A horizons (mol%)																
0.3	15.0	6.3	2.6	13.6	3.8	8.8	11.2	1.9	0.4	6.4	5.6	9.1	3.1	12.3	100.0	—	—
20	15.4	6.7	5.2	16.2	4.5	7.6	9.4	5.7	0.6	5.8	8.6	7.8	2.4	4.1	100.0	—	—
150	15.2	5.7	5.4	16.2	3.2	6.8	8.0	6.0	0.6	4.7	10.0	11.0	2.8	4.2	100.0	—	—
400	16.7	3.3	6.0	15.5	3.6	7.4	8.6	6.7	0.7	4.8	9.3	10.7	2.9	4.0	100.0	—	—
1400	12.7	5.6	5.0	15.6	3.8	8.1	9.4	6.2	0.6	5.6	9.6	9.3	3.4	5.1	100.0	—	—
4100	15.2	7.7	3.4	13.3	5.3	9.2	12.7	3.4	0.4	7.5	5.6	7.2	2.1	7.2	100.0	—	—

(*continued on next page*)

Table 4 (*continued*)

Site age (kyr)	Ala	Val	Thr	Gly	Ile	Pro	Leu	Ser	L-Met	Phe	Asp	Glu	Tyr	Lys	Total	AA-C	AA-N
B horizons (mol%)																	
0.3	13.8	6.8	2.4	12.0	4.2	9.0	10.2	1.4	0.4	6.0	5.9	9.5	2.2	16.0	100.0	—	—
20	15.2	6.7	4.3	14.6	3.3	5.3	6.7	3.7	0.5	3.8	19.2	12.9	0.6	3.2	100.0	—	—
150	13.0	6.5	3.7	12.5	4.0	6.2	8.6	2.9	0.8	5.5	18.0	12.0	1.7	4.7	100.0	—	—
400	14.7	8.1	3.6	13.7	5.7	8.1	11.6	2.8	0.0	6.3	6.7	6.7	1.9	10.1	100.0	—	—
1400	11.8	8.3	2.0	5.5	7.4	10.0	14.3	0.7	0.0	9.2	3.6	9.2	1.2	16.7	100.0	—	—
4100	17.8	9.8	2.2	8.6	6.0	10.7	14.4	1.0	0.0	7.3	1.1	7.2	1.0	13.1	100.0	—	—

D-enantiomer was either below detection or present at trace amounts (Table EA 3). The variation over time in apparent D/L ratios of selected amino acids in topsoils was minor, with no clear patterns across the mineral gradient (Fig. 10A). Average enantiomer ratios of hydrolyzable amino acids (ΣD-AA/ΣL-AA) in topsoils were fairly constant across sites (Fig. 11). D-enantiomers accounted for less than 10% of amino acids (%D = D-isomer × 100%/D + L-isomers), with D-glutamic acid (6%) and D-alanine (5%) being most prominent. In subsoils, enantiomer ratios were more variable, with those of aspartic acid showing a pronounced maximum at 20–400 kyr (Fig. 10B). After correction for HIR, the D-isomer contribution to specific amino acids was larger in subsoils, with the D-enantiomer contributing most to alanine (14%), aspartic acid (9%), and glutamic acid (7%). Whereas average D/L ratios of hydrolyzable amino acids were invariant in topsoils, those in subsoils tended to be larger at the intermediate-aged sites, mainly due to the large abundance of D-aspartic acid (up to 21.5% at Kohala; D/L = 0.274). Across all samples, the D/L ratio of alanine correlated with oxalate-extractable Al ($r = 0.59$; $p < 0.05$), that of aspartic acid with oxalate-extractable Al and Si ($r = 0.96$ and $r = 0.97$; $p < 0.001$); the D/L ratio of lysine correlated with oxalate-extractable Fe + Al ($r = 0.75$; $p < 0.01$), Al ($r = 0.72$; $p < 0.01$) and Si ($r = 0.63$; $p < 0.05$) ($n = 12$). The apparent D/L ratio of alanine correlated negatively to both, the GlcN/MurA ratio (Fig. 5C) and ^{14}C abundance (Fig. 12), respectively. D/L ratios of other amino acids such as lysine, aspartic acid and glutamic acid showed no relation to $\Delta^{14}C$.

3.6. Hydrolyzable amino acids in extraction residues

Following NaOH–NaF extraction, 11 ± 4% of residual ON and 2 ± 1% of residual OC were found with hydrolyzable amino acids ($n = 12$). Their concentration patterns matched those of the non-extracted samples, i.e., least amino acids were present at the youngest (0.3 kyr) and oldest (1400 and 4100 kyr) sites and a maximum occurred at the intermediate-aged sites (Table 4). There were only minor shifts in the abundance of hydrolyzable amino acids in strongly mineral-bound OM when compared with bulk OM. Only the non-extractable amino acid fraction of organic–mineral associations of A horizons at the 20–400-kyr sites contained a larger portions of acidic amino acids (Asp + Glu), which was less clearly pronounced for the non-extracted samples (Fig. 4D).

4. DISCUSSION

4.1. Distribution and dynamics of mineral-associated organic matter and nitrogenous components

4.1.1. A horizons

The modern ^{14}C signature (except for the 20 and 4100-kyr sites) accords with modern ^{14}C ages found for other heavy soil density fractions (Kögel-Knabner et al., 2008). The modern ^{14}C at the 0.3 kyr site can be explained by ongoing accumulation of fresh OM because the sorption capacity of minerals has not yet been reached. This assump-

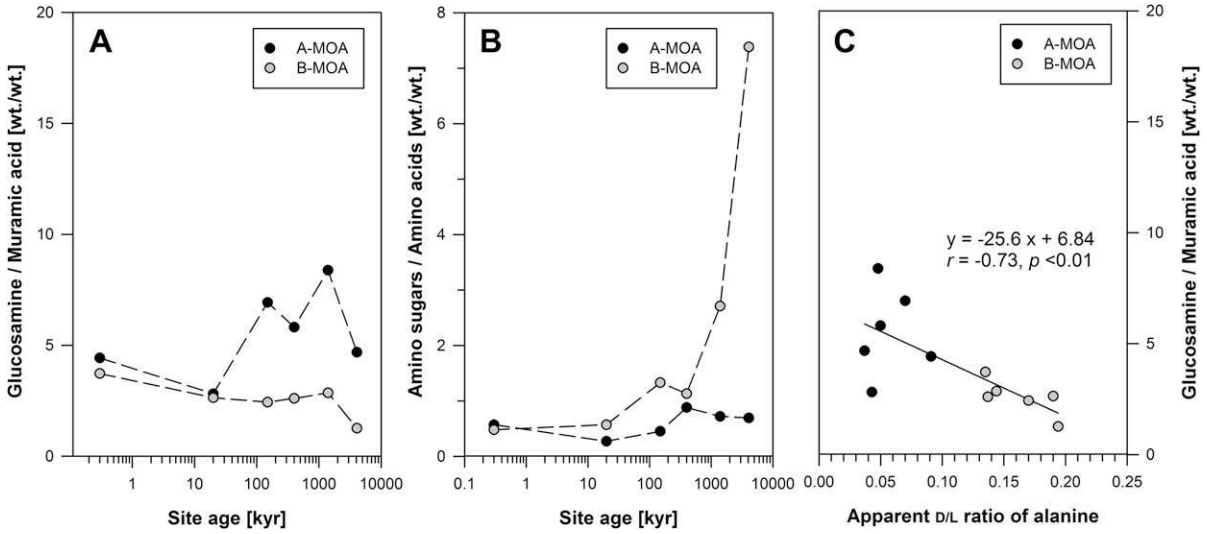

Fig. 5. (A) Glucosamine to muramic acid ratio, (B) ratio of hydrolyzable amino sugars to amino acids, and (C) relationship between the glucosamine to muramic acid ratio and the apparent D/L ratio of alanine in mineral–organic associations from A horizons (A-MOA) and B horizons (B-MOA) across the Hawaiian long substrate age gradient.

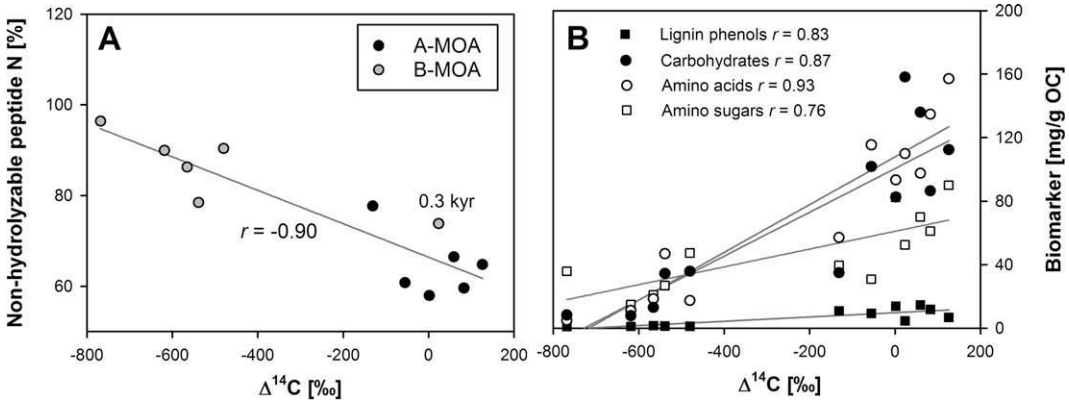

Fig. 6. Relation between the ^{14}C activity and (A) the percentage of estimated non-hydrolyzable peptide N in mineral–organic associations from A horizons (A-MOA) and B horizons (B-MOA) and (B) the OC-normalized concentration of selected biomarkers. Calculated regression functions were: non-hydrolyzable peptide N: $y = 66.49 - 0.037$ x; lignin phenols: $y = 9.7 + 0.01\ x$; carbohydrates: $y = 100.6 + 0.14\ x$; amino acids: $y = 107.9 + 0.15\ x$; amino sugars $y = 61.0 + 0.06\ x$.

tion agrees with the fast incorporation of ^{14}C-labeled OM into the >2-g/cm^3 fraction of an Inceptisol (Swanston et al., 2005). The 400-kyr site contains 290 mg OC/g or ~580 g OM/g, which is similar to the maximum sorption of even the most sorptive mineral phases such as ferrihydrite (Kaiser et al., 2007). Here, in addition to adsorption, coprecipitation with monomeric/polymeric metals seems to contribute to the mineral-associated OM (Mikutta et al., 2009). Precipitation is not likely at the 4100-kyr site where the OM concentration declined in response to the change in mineral composition (Mikutta et al., 2009). The almost entirely modern ^{14}C signature in the topsoil suggests continuous displacement of mineral-associated by fresh OM. Similarly, data by Paul et al. (2008) show that in non-andic and andic surface soils, *ca.* 50% of mineral-associated OC was displaced by fresh OC within a period of 35–50 years. The small apparent D/L ratio of lysine and the constant sum of D-enantiomers (Fig. 11) also imply continuous replenishment of proteinous material in topsoil mineral–organic associations. Interactions of OM with mineral phases in the biologically active upper soil horizons, thus, seem rather dynamic and involve exchange processes. Displacement, thus, can counter the sorption-induced retardation of microbial decomposition as a factor in long-term stabilization of OM (Mikutta et al., 2007; Kalbitz and Kaiser, 2008). Alkaline NaOH–NaF is a strong extractant of OM because of its capability of releasing even strong chemical bonds between OM and mineral constituents due to high pH and displacement of complexed organic functionalities for OH^- and F^-. Non-extractable OM was depleted in ^{14}C, suggesting strongly mineral-bound OM to be older. This is in line with the increased D/L ratios of

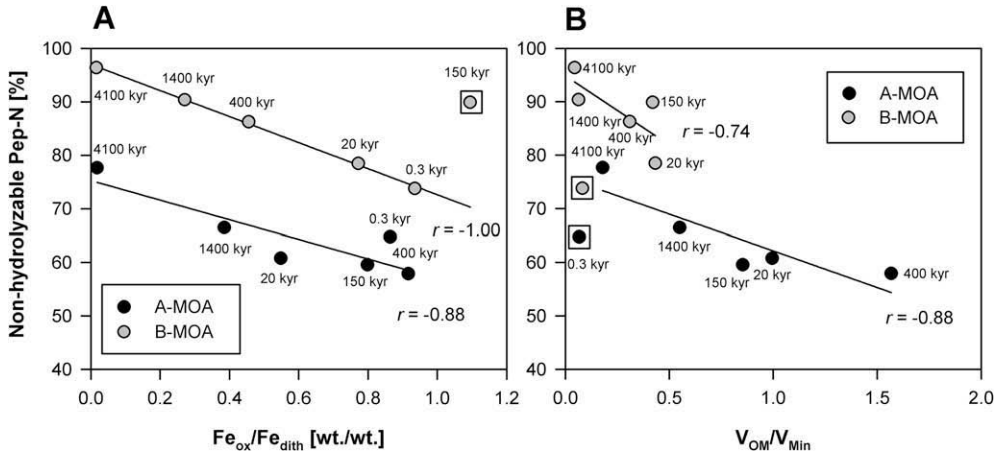

Fig. 7. Relation between the fraction of non-hydrolyzable peptide N with (A) the ratio of oxalate- to dithionite-extractable Fe and (B) the volumetric ratio of OM and minerals in mineral–organic associations from A horizons (A-MOA) and B horizons (B-MOA). The volumetric ratio was calculated as described in Mikutta et al. (2009) assuming an OM density of 1.7 g/cm^3. Samples marked with a square were not included in the regression analysis.

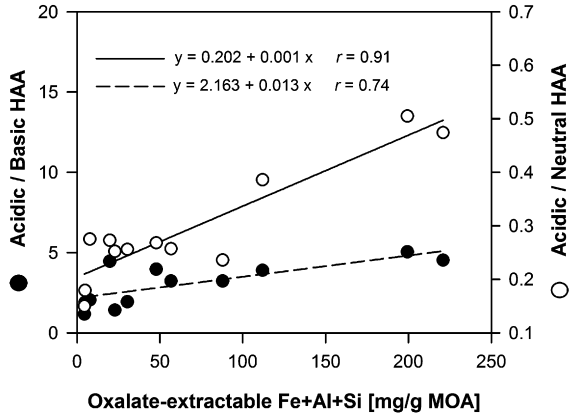

Fig. 8. Relation between the concentration of oxalate-extractable Fe + Al + Si and the (Asp + Glu)/Lys ratio and the (Asp + Glu)/ΣNeutral amino acid ratio where HAA refers to hydrolyzable amino acids and neutral amino acids refer to the sum of alanine, valine, threonine, glycine, isoleucine, proline, leucine, serine, phenylalanine, L-methionine, and tyrosine.

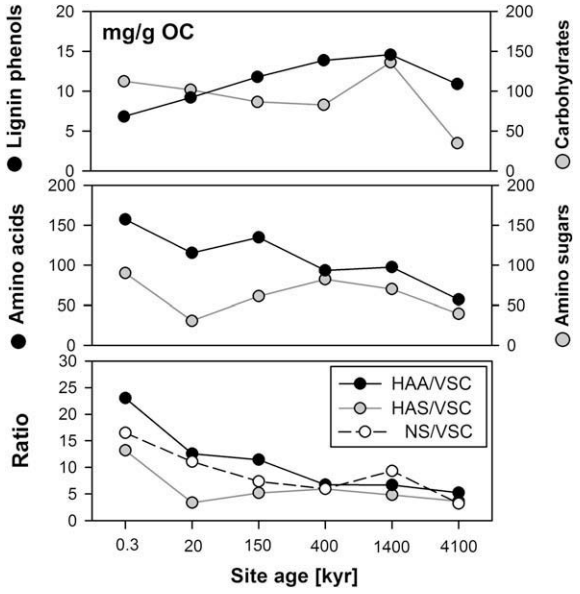

Fig. 9. Carbon-normalized concentrations of lignin phenols, non-cellulosic carbohydrates, amino acids, and amino sugars in mineral–organic associations of A horizons across the Hawaiian long substrate age gradient. The lower panel reveals biomarker ratios of the OC-normalized concentrations of hydrolyzable amino sugars (HAS), amino acids (HAA), neutral sugars (NS), and lignin phenols (VSC). Carbohydrate and lignin data were taken from Mikutta et al. (2009).

bacterial amino acids as well as of lysine in the extraction residues (Table EA 3), indicating that the strongly mineral-bound proteins are more aged than the extractable ones.

4.1.2. B horizons

In contrast to the surface horizons, the mineral–organic associations are ^{14}C-depleted. Mean residence time increases with depth because of the time required to transport OM into deeper horizons (Kalbitz and Kaiser, 2008) and the slower decomposition in subsoil due to limited O_2 availability, less heterotrophic biomass, and stronger mineral–organic interactions (Mikutta et al., 2009). The higher ratio of total D-enantiomers to total L-enantiomers in subsoil than in topsoil mineral–organic associations, the peak in total D-enantiomers at 20–150-kyr sites, and the close positive correlation between D/L ratios of alanine, aspartic acid, and lysine, with oxalate-extractable Al, Fe, and Si suggest that subsoil mineral–organic associations contain aged proteins, likely because of effective stabilization of OM with poorly crystalline mineral phases. The accumulation of aspartic acid during 20 and 150 kyr, in conjunction with its elevated apparent D/L ratio, can be interpreted as preferential mineral-induced stabilization of acidic proteins. However, since soils are chromatographic systems where OM is gradually transported into deeper soil horizons (Kalbitz and Kaiser, 2008), the elevated D/L ratios can also be caused by

Table 5
Concentration and composition of hydrolyzable amino sugars (AS) in organic soil layers and mineral–organic associations along the Hawaiian long substrate age gradient. *Abbreviations:* GlcN, glucosamine; ManN, mannosamine; GalN, galactosamine; MurA, muramic acid; AS-C, C in hydrolyzable amino sugars; AS-N, N in hydrolyzable amino sugars.

Site age (kyr)	GlcN	ManN	GalN	MurA	Total	AS-C	AS-N	GlcN/MurA	GlcN/GallN
Organic soil layers									
						(%)	(%)	(wt./wt.)	(wt./wt.)
L horizons (μmol/g)									
0.3	6.5	3.2	2.3	4.4	16.4	0.5	3.4	1.5	2.9
20	20.1	9.3	12.3	3.8	45.4	1.4	5.3	5.3	1.6
150	9.9	3.7	3.0	1.5	18.2	0.6	3.0	6.4	3.3
400	20.6	4.9	8.5	1.9	35.8	1.1	4.3	11.1	2.4
1400	16.1	2.7	2.8	1.6	23.3	0.7	3.7	9.9	5.8
4100	7.4	2.1	2.0	1.2	12.8	0.4	3.0	6.1	3.6
O horizons (μmol/g)									
0.3	58.3	5.3	28.3	4.9	96.8	3.4	8.1	12.0	2.1
20	71.1	5.9	24.8	6.8	108.7	4.0	7.2	10.4	2.9
150	49.3	3.6	19.6	4.9	77.4	3.4	6.4	10.0	2.5
400	66.7	5.3	27.4	6.1	105.4	3.3	6.3	10.9	2.4
1400	61.3	5.9	26.6	4.6	98.4	4.0	8.0	13.5	2.3
4100	76.3	5.8	28.3	9.4	119.9	4.5	9.8	8.1	2.7
L horizons (mol%)									
0.3	39.8	19.8	13.8	26.6	100.0	—	—	—	—
20	44.2	20.4	27.2	8.3	100.0	—	—	—	—
150	54.5	20.6	16.4	8.5	100.0	—	—	—	—
400	57.5	13.6	23.7	5.2	100.0	—	—	—	—
1400	69.2	11.8	12.0	7.0	100.0	—	—	—	—
4100	58.1	16.3	16.1	9.6	100.0	—	—	—	—
O horizons (mol%)									
0.3	60.2	5.5	29.3	5.0	100.0	—	—	—	—
20	65.4	5.4	22.8	6.3	100.0	—	—	—	—
150	63.7	4.7	25.3	6.3	100.0	—	—	—	—
400	63.2	5.0	26.0	5.8	100.0	—	—	—	—
1400	62.3	6.0	27.1	4.6	100.0	—	—	—	—
4100	63.7	4.9	23.6	7.8	100.0	—	—	—	—
Mineral–organic associations									
A horizons (μmol/g MOA)									
0.3	4.9	0.5	2.9	0.8	9.1	8.3	5.6	4.4	1.7
20	14.6	1.5	9.2	3.7	29.0	2.9	4.1	2.8	1.6
150	33.9	4.2	21.0	3.5	62.5	5.6	6.6	6.9	1.6
400	71.1	6.9	43.2	8.7	129.9	7.6	9.4	5.8	1.6
1400	32.3	2.2	12.9	2.8	50.1	6.5	7.2	8.4	2.5
4100	5.6	0.1	1.8	0.9	8.5	3.7	4.2	4.7	3.1
B horizons (μmol/g MOA)									
0.3	3.57	0.3	1.9	0.7	6.5	4.8	3.6	3.7	1.8
20	7.52	0.8	5.8	2.0	16.2	2.5	4.0	2.6	1.3
150	4.13	0.3	3.9	1.2	9.5	1.4	3.0	2.4	1.1
400	4.66	0.2	2.8	1.3	8.9	1.9	3.5	2.6	1.7
1400	2.22	0.1	2.1	0.6	5.0	4.4	3.5	2.9	1.0
4100	0.78	0.5	0.6	0.4	2.2	3.3	1.9	1.3	1.4
A horizons (mol%)									
0.3	54.4	5.5	31.4	8.8	100.0	—	—	—	—
20	50.4	5.1	31.7	12.8	100.0	—	—	—	—
150	54.1	6.7	33.6	5.6	100.0	—	—	—	—
400	54.7	5.3	33.3	6.7	100.0	—	—	—	—
1400	64.5	4.4	25.6	5.5	100.0	—	—	—	—
4100	66.7	1.4	21.7	10.2	100.0	—	—	—	—
B horizons (mol%)									
0.3	54.7	5.3	29.6	10.5	100.0	—	—	—	—
20	46.6	5.1	35.7	12.6	100.0	—	—	—	—

(*continued on next page*)

Table 5 (*continued*)

Site age (kyr)	GlcN	ManN	GalN	MurA	Total	AS-C	AS-N	GlcN/MurA	GlcN/GallN
150	43.6	2.7	40.9	12.8	100.0	—	—	—	—
400	52.2	2.3	31.3	14.3	100.0	—	—	—	—
1400	44.1	2.4	42.5	11.0	100.0	—	—	—	—
4100	35.0	19.9	25.3	19.8	100.0	—	—	—	—

microbial utilization of the L-enantiomer during the downward migration of proteinous OM. Microbial processing of marine dissolved OM, for example, caused a substantial increase in D/L ratios of aspartic acid, alanine, and glutamic acid within only 219 h (Amon et al., 2001). Irrespective of the cause, the subsoil D/L ratios suggest the presence of 'aged' proteins. Based on the increase in lysine D/L ratios and in ^{14}C ages from topsoil to subsoil, we estimated the racemization rate of lysine (K_{rac}) of the six sites to between 3×10^{-5}/yr and 3×10^{-7}/yr (at 288 K), which is comparable to values calculated for British upland soils (Amelung et al., 2006). However, there is no relationship between the ^{14}C age and the D/L ratio of lysine, which contrasts previous findings (Amelung, 2003). The D/L ratio of lysine in subsoil mineral–organic associations of the 0.3-kyr site (D/L = 0.012; $\Delta^{14}C = 24‰$) was similar to that of the 4100-kyr site (D/L = 0.011; $\Delta^{14}C = -768‰$). Consequently, age dating of proteinous ON based on lysine enantiomers is impossible for the study sites. Also the decrease in ^{14}C activity with depth was not correlated with the increase in amino acid D/L ratios, suggesting unique biogeochemical dynamics at each site. For proline, valine, leucine, isoleucine, and phenylalanine, we observed no or only little D-forms, indicating minor racemization. The reason for the contrasting findings, i.e., the formation of D-lysine and the absence of D-enantiomers of others amino acids, is unclear. Possibly, certain amino acids are not prone to racemization because of their position within the protein structure as racemization is faster for terminal amino acids than for amino acids at internal positions (Bada, 1984). Also linkages of amino acids to other OM components may slow racemization (Rafalska et al., 1991).

The partial extraction of older OM by NaOH–NaF seems linked to the dissolution of Al, Si and Fe phases under alkaline conditions. However, the fact that the D/L ratio of lysine in subsoil mineral–organic associations increased after NaOH–NaF extraction, confirms that strongly bound proteins resist stronger against biodegradation than weakly attached ones.

In summary, stabilization of mineral-associated proteinous OM in surface horizons is weaker than in the deeper soil. In subsoils, stabilization is more effective in presence of poorly crystalline minerals.

4.2. Nitrogen species at particle surfaces

XPS and N K-edge NEXAFS analyses confirmed that most mineral-bound ON was in peptide structures, with only minor differences between top– and subsoils. This is line with previous studies, showing amide N to be the dominant ON form in soils and sediments (Knicker, 2004; Abe et al., 2005). According to XPS analyses of powder samples, aromatic N contributed 18–34% to mineral-bound ON. This is at the upper end of the range reported in XPS and NEXAFS studies of humic substances (3–30%; Vairamurthy and Wang, 2002; Abe and Watanabe, 2004; Abe et al., 2005). Heterocycle N has been found in cultivated soils (Leinweber et al., 2009), seawater dissolved OM (Maie et al., 2006), and in marine sediments (Patience et al., 1992). Black carbon generated during vegetation fires, plant or microbial DNA and RNA or their fragments (Levy-Booth et al., 2007), and plant-derived alkaloids (Somei and Yamada, 2004) are possible sources of aromatic N. Vairamurthy and Wang (2002) suggest that pyridine N might be formed by reaction of NH_4^+ with carbonyl groups of phenolic lignin degradation products or related compounds. The large abundance of aromatic C in the study samples supports this scenario. The covariation of aromatic C and aromatic N ($r = 0.91$; $n = 12$), combined with results obtained from of Ar^+ sputtering (Mikutta et al., 2009), suggests that aromatic N is concentrated in closer proximity of mineral surfaces, probably as part of strongly sorbing OM (Kaiser et al., 2001; Kawahigashi et al., 2006). Tight association of the strongly sorbing OM with mineral surfaces and hence its restricted extractability could consequently explain why NaOH–NaF-extractable OM had relatively little heterocycle N.

4.3. Bacterial versus fungal contribution to mineral-associated organic N

The hydrolyzable amino acid and amino sugar data suggest microbial residues to be important contributors to mineral-associated ON, accounting for, at least, 14–31% of total N in topsoils and 2–17% of total N in subsoils. Their hydrolytic release from aged mineral–organic associations ($\Delta^{14}C < -450‰$) indicates effective mineral-induced stabilization, especially in subsoils. The larger contribution of amino sugars relative to amino acids at older sites and in subsoils (Fig. 5B) hints at a progressive decomposition state of mineral-bound OM. Typically, microbial decomposition and recycling of amino acids result in the production, thus accumulation of amino sugars (Amelung et al., 2001; Brodowski et al., 2004). Limited sources of easily accessible C and N at older sites and in deep soil might promote efficient resynthesis of microbial necromass.

Compared to the O layers, where the GlcN/MurA ratios reveal a larger abundance of fungal biomass, mineral-associated ON in topsoils comprised more bacterial residues (Table 5). The GlcN/MurA ratios (5.5 ± 2.0) are close to values reported for pure bacteria (2–8; Joergensen et al., 1995; Glaser et al., 2003), hence indicating an almost exclusive bacterial origin of amino sugars. The range of GlcN/MurA ratios is also consistent with those of tropical

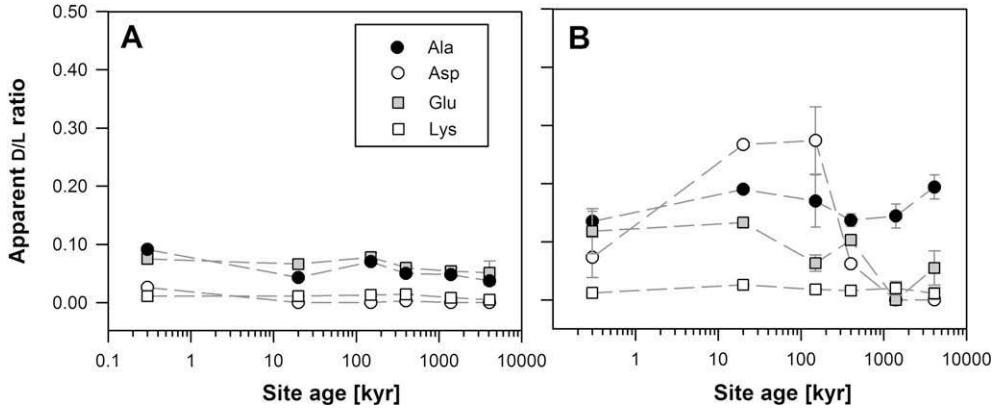

Fig. 10. Apparent D/L ratios of selected hydrolyzable amino acids in mineral–organic associations of (A) A horizons and (B) B horizons across the Hawaiian long substrate age gradient. *Abbreviations:* Ala, alanine; Asp, aspartic acid + asparagine; Glu, glutamic acid + glutamine; Lys, lysine.

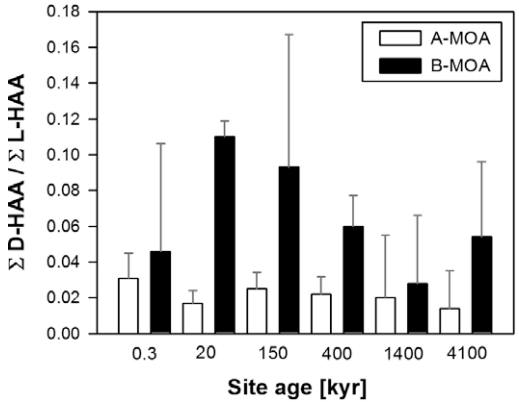

Fig. 11. Apparent ratio of total D-enantiomers to total L-enantiomers of hydrolyzable amino acids (HAA) in mineral–organic associations of A horizons (A-MOA) and B horizons (B-MOA) across the Hawaiian long substrate age gradient. *Note:* the large error bars result from error propagation including analytical errors and errors from calculating the D/L ratios of individual amino acids as well as from addition of the individual D/L ratios.

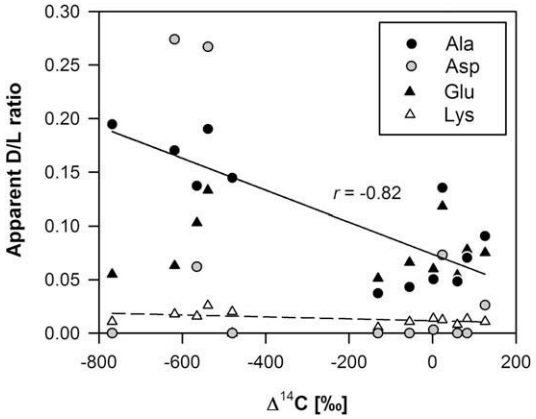

Fig. 12. Relationship between the ^{14}C activity and the apparent D/L ratios of hydrolyzable amino acids in mineral–organic associations across the Hawaiian long substrate age gradient. The D/L ratio of lysine, an age marker for proteinous ON, does not change markedly with ^{14}C activity (dashed line). The significant relationship between the D/L ratio of alanine and ^{14}C activity predominantly reflects differences in the D-alanine content of topsoil and subsoil mineral–organic associations, implying a larger microbial contribution in deeper soil.

forest soils developed from sedimentary and ultrabasic rocks under comparable climatic conditions (Moritz et al., 2009). The large contribution of bacterial biomass to mineral-associated ON in topsoils is also confirmed by the high D/L ratios of alanine, aspartic and glutamic acid. These compounds originate mainly from bacterial peptidoglycans. The D/L ratio of alanine, which is negatively correlated to the GlcN/MurA ratio (Fig. 5C), was comparable or even smaller than that of bacteria cultures and commercial peptidoglycans (Amon et al., 2001; Veuger et al., 2007), thus highlighting the role of bacterial source compounds to mineral-associated ON.

The smaller GlcN/MurA ratio (2.6 ± 0.8) in subsoils than in surface horizons suggests an even larger contribution of bacterial residues. This likely is due to reduced O_2 partial pressure in the subsoil, as fungal activity relies on oxic conditions. The larger abundance of muramic acid in deep soil (Table 5) also points at an efficient stabilization of microbial residues since muramic acid, when free, is considered labile (Zhang et al., 1998). While the total concentration of amino sugars, as well as of amino acids, in mineral–organic associations is controlled by shifts in the soil mineral composition (Fig. 4B), there was no evidence for a mineral-induced change in the partitioning of bacterial versus fungal residues as suggested by Moritz et al. (2009).

4.4. Association of peptide N with mineral surfaces

Using Eq. (2), we estimated that *ca.* 58–96% of mineral-bound peptide N escaped hydrolysis. This contrasts the almost quantitative release of mineral-associated ON ($92 \pm 4\%$) upon acid hydrolysis, especially in subsoils. Part of the difference may result from amino acids not included in estimating peptide N, such as ornithine, arginine,

cysteine, α- and γ-aminobutyric acid. However, also the presence of non-hydrolyzable compounds needs to be considered. Abe et al. (2005) showed that peptides comprised the largest fraction of non-hydrolyzable N in humic acids (59–80%). Amide N has also been found in hydrolysis residues of plant materials and sediments (Knicker and Lüdemann, 1995; Knicker and Hatcher, 1997) and of high-molecular weight dissolved OM from marine waters (Aluwihare et al., 2005).

Non-hydrolyzability of amide N typically is explained by stabilization of proteins upon interactions with OM or minerals (Leinweber and Schulten, 2000; Knicker, 2004). The fraction of non-hydrolyzable peptide N was smallest in A horizons of the 20–400-kyr sites, where the poorly crystalline minerals and the volumetric OM–mineral ratios were maximal (Fig. 7A and B). In contrast, non-hydrolyzable N was largest at the older sites (1400 and 4100 kyr), where crystalline secondary Fe minerals dominated and volumetric OM–mineral ratios were much smaller.

There are indications that most peptide compounds are not enriched at particle surfaces but simply contained in mineral-associated OM: (i) the close OC–ON correlation ($r = 0.96$, $n = 12$, $p < 0.001$), (ii) the simultaneous decrease in C and N XPS signals during Ar^+ sputtering, and (iii) the concentration of extractable ON in the aromatic XAD-8 adsorbable fraction (Table 1). Moreover, the large volumetric OM–mineral ratios in A horizons of the 20–400-kyr sites exclude the possibility that all peptide compounds can form direct bonds to mineral surfaces. Therefore, most of peptide N seems to become attached to minerals as an integral part of sorbing OM. Similarly, Kaiser and Zech (2000) observed a proportional uptake of ON and OC to goethite, $Al(OH)_3$, kaolinite, illite, and subsoil material, resulting in approximately constant OC/ON ratios of sorbed OM. Lilienfein et al. (2004) also found no differential sorption of OC and ON to soils from andesitic substrate.

If the conclusion above is valid, the question arises whether the chemically stable peptides are recalcitrant plant-derived compounds, such as protein complexes with tannins, polyphenols, or polysaccharides (Greenfield, 1972), or do form in the organic soil layers. Yu et al. (2000) showed that dissolved ON from organic forest floor layers was primarily in the sorptive hydrophobic OM fraction and related closely to polyphenols, suggesting that much of the ON enters the mineral soil with ON–polyphenol complexes. However, non-hydrolyzable peptide N was minimal at intermediate-aged sites where most ON was with the XAD-8-adsorbable aromatic OM (Table 1). Hence, aromaticity of OM alone cannot explain the hydrolyzability of mineral-bound peptide N. Steric aspects may contribute to the protection of peptide N (Zang et al., 2000).

Across all samples, non-hydrolyzable peptide N linearly increased with ^{14}C age irrespective of differences in OM sources (Fig. 6A). This indicates that older OM in subsoil comprises a larger fraction of chemically stable peptide N which is in agreement with the larger amount of amino acid D-enantiomers in the subsoils. The increase of non-hydrolyzable peptide N with soil depth and subsequently with aged OM went along with a decrease in detectable biomarker molecules (Fig. 6B). Aromatic C in topsoils and subsoils, as revealed by XPS, were similar but CuO-derived lignin phenols in subsoil were an order of magnitude less than in topsoil (Mikutta et al., 2009). We, therefore, hypothesize alterations during the progressive transport into deeper horizons that cause the decrease in identifiable compounds and also contribute to resistance of peptide N to hydrolysis. The significant linear correlation between non-hydrolyzable peptide N and mean horizon depth supports the idea. The close correlation of non-hydrolyzable peptide N and the crystallinity of Fe oxides (Fig. 7A) offers another possible explanation. While association with poorly crystalline minerals seems to promote the initial accumulation and stabilization, the binding to crystalline hydrous Fe oxides allows for nitrogenous (and other organic) matter to survive longer, probably due to preferential uptake of inherently stable compounds.

In summary, ON appears to associate with soil minerals as part of sorbing OM. Topsoils rich in poorly crystalline mineral phases tend to accumulate more chemically labile peptide N. In turn, subsoils with crystalline Fe oxides, while not as effective as poorly crystalline mineral phases in total OM accumulation, retain compounds either structurally or sterically less prone to hydrolytic digestion or embedded in other compounds, thus protected from hydrolytic attack. This means the extent to which certain minerals impact the accumulation and stabilization of nitrogenous compounds depends on their (i) overall sorption capacity and (ii) on their selectivity for compounds of different chemical and biological stability.

4.5. Variations in organic N content and composition with changing mineral assemblage

Patterns of N-containing biochemical compounds within mineral-associated OM differ strongly along the weathering gradient and from those of the organic layers, highlighting the effects of interactions of OM with minerals (Fig. 9; Mikutta et al., 2009). Retention by primary silicates seems largely non-selective (youngest site). In contrast, poorly crystalline mineral phases of variable charge (e.g., allophane and secondary Fe and Al (hydr)oxides) are highly selective for lignin-derived phenols (intermediate age sites). In result, mineral–organic associations at the youngest site contain a larger portion of microbial residues rich in N while older sites appear to hold more plant-derived, N-poor lignin residues (Fig. 9). This finding also matches the larger OC/ON ratios at the 20–400-kyr sites (Table 1), which are in line with sorption and precipitation experiments, showing that poorly crystalline Al (hydr)oxides as well as Al–OM precipitates, although binding much OM, preferentially retain N-depleted OM (Kaiser and Zech, 2000; Scheel et al., 2008).

The amino acid pattern also reveals a distinct mineral effect. As compared with the overlying O horizons, acidic amino acids (aspartic and glutamic acid) were similarly or more abundant in mineral horizons at the 20–400-kyr sites but depleted at the youngest and the oldest site. The trend was more pronounced for subsoils than for topsoils (Table 4

and Fig. 4D). This suggests carboxyl-rich proteins to associate more with poorly crystalline minerals and less well with primary and secondary aluminosilicate minerals (e.g., pyroxene, kaolinite, and halloysite). These minerals, due their permanent negative charge, retain more proteins containing a larger density of cationic (protonated) amino groups. The close relationship of oxalate-extractable Fe, Al, and Si to acidic amino acids (Fig. 8) underlines the preferential association with poorly crystalline mineral phase, which are positively charged under the given acidic soil conditions.

The observed distribution pattern of acidic and basic amino acids fit well to results of sorption experiments with individual amino acids and peptides. Variable-charge minerals such as ferrihydrite retain preferentially acidic amino acids (Matrajt and Blanot, 2004), while negatively charged aluminosilicates favor basic amino acids and peptides (Dashman and Stotzky, 1984; Keil et al., 1998; Aufdenkampe et al., 2001). The differential accumulation of biocompounds along the weathering gradient together with the shifts in amino acid composition suggest that sorptive fractionation of OM, induced by the different mineral assemblages, is an important factor in controlling the distribution, accumulation and stabilization of N-containing biocompounds in soil.

As outlined above, there is evidence that most ON enters mineral–organic associations as an integral component of sorbing OM. How does that fit to the mineral-specific variation in composition of proteineous material? Proteinous material in all samples was dominated by neutral amino acids, with minor portions of acidic and basic ones. Nevertheless, these compounds seem to affect the interaction with minerals, probably by adding to the overall charge of the sorbing OM when at exposed positions. This assumption is in line with the finding that sorption of melanoidins to clays depends on the charge properties of the contained amino acids (Hedges, 1978). Here, more research is needed to evaluate the significance of this model in the sorptive retention of proteins in soils.

5. SUMMARY AND IMPLICATIONS

This study evidences that the soil mineral composition significantly affects the N cycling in soils by controlling the amount and chemical composition of soil ON (Fig. 13). Sites enriched in poorly crystalline minerals, which form upon weathering of basaltic tephra, retained more ON than the youngest and oldest sites comprising either primary minerals (olivine, pyroxene, feldspar) or secondary Fe oxides and kaolin clays. The concentration of

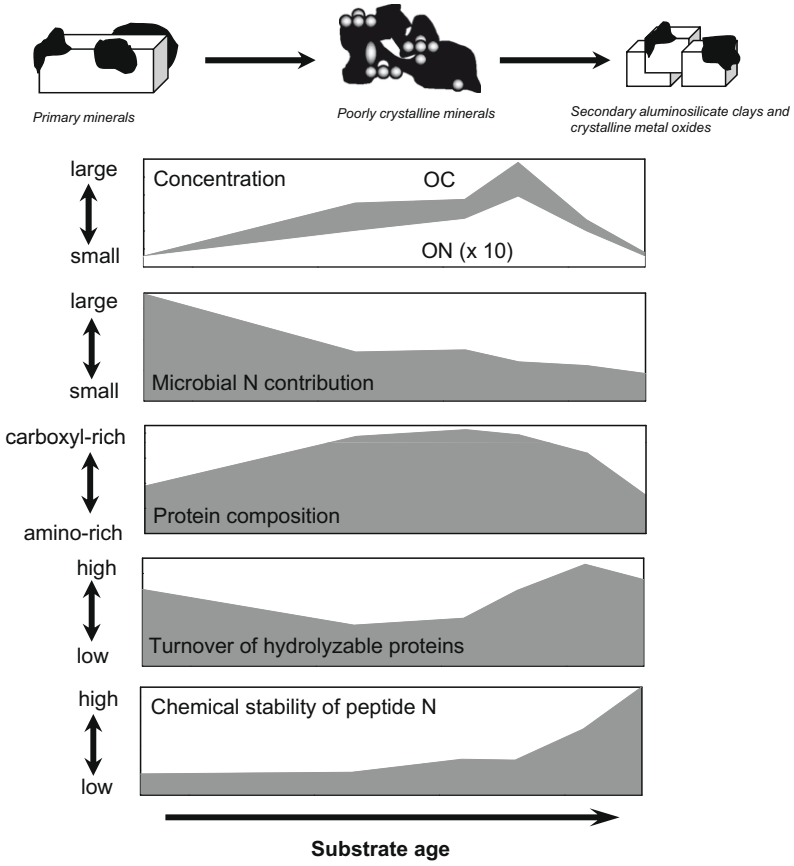

Fig. 13. Generalized scheme of the time-dependent alteration of organic N (ON) in mineral–organic associations across the Hawaiian long substrate age gradient. *Note:* most measured ON properties refer to N compounds susceptible to acid hydrolysis. In contrast, chemical stability refers to peptide N resistant against hydrolytic attack.

mineral-associated ON (amino acids, amino sugars) closely matched trends in OC accumulation, suggesting that most ON binds to minerals as part of sorbing OM. The differential affinity of N-rich and N-poor compounds (non-cellulosic carbohydrates, amino acids, amino sugars, lignin phenols) for certain mineral phases results in shifts in OC/ON ratios of mineral-bound OM, with the youngest site holding more microbial-derived N compounds. The hydrolyzable part of mineral-bound ON in A horizons, being largest at sites with poorly crystalline minerals, is primarily of bacterial origin and turns over quickly irrespective of the mineral assemblage. In deeper soil, the smaller portion of hydrolyzable ON, with an even larger microbial contribution, went along with the presence of older proteins. Subsoil horizons rich in poorly crystalline minerals more effectively stabilize acidic protein structures. Proteinous N in OM directly bound to soil minerals was enriched in acidic amino acids and appears more stabilized, whereas weakly bonded N compounds seem more bioavailable.

Irrespective of the mineral assemblage, most mineral-associated ON is acid soluble but escapes hydrolysis, likely because of integration of peptide material within chemically stable OM structures. The poorly hydrolyzable peptide N in topsoil mineral–organic associations, containing young OM, may previously form in the overlying forest floor layers and subsequently be leached into the mineral soil beneath. Being attached to other organic structures, peptide compounds migrate down into the deeper soil. This seems accompanied by a progressive enrichment of more non-hydrolyzable peptide N, likely caused by the microbial utilization of more labile components. Mineral–OM interactions may thus decrease the availability of ON for microorganisms and plants particularly in subsoils. As result, minerals may accentuate N limitation especially at the 0.3-kyr site (Vitousek, 2004). At older sites, holding more mineral-associated ON, N is not limited, likely because ON components (amino acids and amino sugars) are less strongly bound to variable-charge minerals and, thus, remain accessible to microorganisms. Consequently, mineral–organic associations appear actively involved in the cycling of ON (as of OC), depending on the mineral assemblage, influencing the N nutrition status of ecosystems. We propose that the N dynamics at the ecosystem level is not only affected by microbial–plant interactions but includes mineral–organic feedbacks.

ACKNOWLEDGMENTS

We are grateful to Peter Vitousek for his leadership in the Hawaiian Ecosystem Research and to Heraldo Farrington for his enthusiastic support during sampling. For the XPS analyses we appreciate the support of Marion Bertram (GWT-TUD GmbH); for laboratory assistance we are thankful to Heike Oetzmann, Gerlinde Hardt, and Christine Krenkewitz. Financial support was provided by the German Research Foundation (DFG project Gu 406/18-1). Sampling support for Marc Kramer was provided by the USDA CSREES NR1 program 2007-03184. We also appreciate the comments of Jay Brandes and of three anonymous reviewers.

APPENDIX A. SUPPLEMENTARY DATA

Supplementary data associated with this article can be found, in the online version, at doi:10.1016/j.gca.2010.01.006.

REFERENCES

Abe T., Maie N. and Watanabe A. (2005) Investigation of humic acid N with X-ray photoelectron spectroscopy: effect of acid hydrolysis and comparison with ^{15}N cross polarization/magic angle spinning nuclear magnetic resonance spectroscopy. *Org. Geochem.* **36**, 1490–1497.

Abe T. and Watanabe A. (2004) X-ray photoelectron spectroscopy of nitrogen functional groups in soil humic acids. *Soil Sci.* **169**, 35–43.

Aiken G. R. and Leenheer J. A. (1993) Isolation and chemical characterization of dissolved and colloidal organic matter. *Chem. Ecol.* **8**, 135–151.

Aluwihare L. I., Repeta D. J., Pantoja S. and Johnson C. G. (2005) Two chemically distinct pools of organic nitrogen accumulate in the ocean. *Science* **308**, 1007–1010.

Amelung W., Zhang T. X. and Flach K. W. (2006) Amino acids in grassland soils: climatic effects on concentrations and chirality. *Geoderma* **130**, 207–217.

Amelung W. (2003) Nitrogen biomarkers and their fate in soil. *J. Plant Nutr. Soil Sci.* **166**, 677–686.

Amelung W. and Brodowski S. (2002) In vitro quantification of hydrolysis-induced racemization of amino acid enantiomers in environmental samples using deuterium labeling and electron-impact ionization mass spectrometry. *Anal. Chem.* **74**, 3239–3246.

Amelung W., Miltner A., Zhang X. and Zech W. (2001) Fate of microbial residues during litter decomposition as affected by minerals. *Soil Sci.* **166**, 598–606.

Amon R. M. W., Fritznar H.-P. and Benner R. (2001) Linkages among the bioreactivity, chemical composition, and diagentic state of marine dissolved organic matter. *Limnol. Oceanogr.* **46**, 287–297.

Aufdenkampe A. K., Hedges J. I., Richey J. E., Krusche A. V. and Lierena C. A. (2001) Sorptive fractionation of dissolved organic nitrogen and amino acids onto fine sediments within the Amazon Basin. *Limn. Oceanogr.* **46**, 1981–1985.

Bada J. L. (1984) In vivo racemization in mammalian proteins. *Methods Enzymol.* **106**, 98–115.

Blakemore L. C., Searle P. L. and Daly B. K. (1987) Methods for Chemical Analysis of Soils. *New Zealand Soil Bureau Scientific Report 80*. NZ Soil Bureau, Department of Scientific and Industrial Research, Lower Hutt, New Zealand.

Brodowski S., Amelung W., Lobe I. and du Preez C. C. (2004) Losses and biogeochemical cycling of soil organic nitrogen with prolonged arable cropping in the South African Highveld—evidence from D- and L-amino acids. *Biogeochemistry* **71**, 17–42.

Chorover J., Amistadi M. K. and Chadwick O. A. (2004) Surface charge evolution of mineral–organic complexes during pedogenesis in Hawaiian basalt. *Geochim. Cosmochim. Acta* **68**, 4859–4876.

Dashman T. and Stotzky G. (1984) Adsorption and binding of peptides on homoionic montmorillonite and kaolinite. *Soil Biol. Biochem.* **16**, 51–55.

Espeland E. M. and Wetzel R. G. (2001) Complexation, stabilization, and UV photolysis of extracellular and surface-bound glucosidase and alkaline phosphatase: implications for biofilm microbiota. *Microb. Ecol.* **42**, 572–585.

Fan T. W.-M., Lane A. N., Chekmenev E., Wittebort R. J. and Higashi R. M. (2004) Synthesis and physico-chemical properties of peptides in soil humic substances. *J. Peptide Res.* **63**, 253–264.

Fu Q., Wan W., Hu H. and Chen S. (2008) Adsorption of the insecticidal protein of *Bacillus thuringiensis* subsp. *Kurstaki* by minerals: effect of inorganic salts. *Eur. J. Soil Sci.* **59**, 216–221.

Glaser B., María-Belén T. and Kassem A. (2003) Amino sugars and muramic acid—biomarkers for soil microbial community structure analysis. *Soil Biol. Biochem.* **36**, 399–407.

Gleixner G., Poirier N., Bol R. and Balesdent J. (2002) Molecular dynamics of organic matter in a cultivated soil. *Org. Geochem.* **33**, 357–366.

Greenfield L. G. (1972) The nature of the organic nitrogen of soils. *Plant Soil* **136**, 191–198.

Guggenberger G., Frey S. D., Six J., Paustian K. and Elliott E. T. (1999) Bacterial and fungal cell-wall residues in conventional and no-tillage agroecosystems. *Soil Sci. Soc. Am. J.* **63**, 1188–1198.

Hedges J. I. (1978) The formation and clay mineral reactions of melanoidins. *Geochim. Cosmochim. Acta.* **42**, 69–76.

Hesse R., Chassé T. and Szargan R. (2003) Unifit 2002—universal analysis software for photoelectron spectra. *Anal. Bioanal. Chem.* **375**, 856–863.

Hsu P.-H. and Hatcher P. G. (2005) New evidence for covalent coupling of peptides to humic acids based on 2D NMR spectroscopy: a means for preservation. *Geochim. Cosmochim. Acta* **69**, 4521–4533.

Joergensen R. G., Scholle G. and Wolters V. (1995) Die Bestimmung von Muraminsäure als Biomarker von Bakterien. *Mitt. Dtsch. Bodenkund. Ges.* **76**, 627–630.

Juo A. S. R. and Kamprath E. J. (1979) Copper chloride as an extractant for estimating the potentially reactive aluminum pool in acid soils. *Soil Sci. Soc. Am. J.* **43**, 35–38.

Kaiser K. and Zech W. (2000) Sorption of dissolved organic nitrogen to by acid subsoil horizons and individual mineral phases. *Eur. J. Soil Sci.* **51**, 403–411.

Kaiser K., Mikutta R. and Guggenberger G. (2007) Increased stability of organic matter sorbed to ferrihydrite and goethite on aging. *Soil Sci. Soc. Am. J.* **71**, 711–719.

Kaiser K., Guggenberger G. and Zech W. (2001) Isotopic fractionation of dissolved organic carbon in shallow forest soils as affected by sorption. *Eur. J. Soil Sci.* **52**, 585–597.

Kalbitz K. and Kaiser K. (2008) Contribution of dissolved organic matter to carbon storage in forest mineral soils. *J. Plant Nutr. Soil Sci.* **171**, 52–60.

Kalbitz K., Schwesig D., Rethemeyer J. and Matzner E. (2005) Stabilization of dissolved organic matter by sorption to the mineral soil. *Soil Biol. Biochem.* **37**, 1319–1331.

Kawahigashi M., Kaiser K., Rodionov A. and Guggenberger G. (2006) Sorption of dissolved organic matter by mineral soils of the Siberian forest tundra. *Global Change Biol.* **12**, 1868–1877.

Keil R. G., Tsamakis E., Giddings J. C. and Hedges J. I. (1998) Biochemical distributions (amino acids, neutral sugars, and lignin phenols) among size-classes of modern marine sediments from the Washington coast. *Geochim. Cosmochim. Acta* **62**, 1347–1364.

Knicker H. (2004) Stabilization of N-compounds in soil and organic-matter-rich sediments—what is the difference? *Mar. Chem.* **92**, 167–195.

Knicker H. and Hatcher P. G. (1997) Survival of protein in an organic-rich sediment: possible protection by encapsulation in organic matter. *Naturwissenschaften* **84**, 231–234.

Knicker H. and Lüdemann H.-D. (1995) N-15 and C-13 CPMAS and solution NMR studies of N-15 enriched plant material during 600 days of microbial degradation. *Org. Geochem.* **23**, 329–341.

Kögel-Knabner I. (2002) The macromolecular organic composition of plant and microbial residues as inputs of soil organic matter. *Soil Biol. Biochem.* **34**, 139–162.

Kögel-Knabner I., Guggenberger G., Kleber M., Kandeler E., Kalbitz K., Scheu S., Eusterhues K. and Leinweber P. (2008) Organo-mineral associations in temperate soils: integrating biology, mineralogy, and organic matter chemistry. *J. Plant Nutr. Soil Sci.* **171**, 61–82.

Leinweber P., Kruse J., Walley F. L., Gillespie A., Eckhardt K.-U., Blyth R. I. R. and Regier T. (2007) Nitrogen K-edge XANES—an overview of reference compounds used to identify 'unknown' organic nitrogen in environmental samples. *J. Synch. Rad.* **143**, 500–511.

Leinweber P., Walley F. L., Kruse J., Jandl G., Eckhardt K.-U., Blyth R. I. R. and Regier T. (2009) Cultivation affects soil organic nitrogen: pyrolysis-mass spectrometry and nitrogen K-edge XANES spectroscopy evidence. *Soil Sci. Soc. Am. J.* **73**, 82–92.

Leinweber P. and Schulten H.-R. (2000) Nonhydrolyzable forms of soil organic nitrogen: extractability and composition. *J. Plant Nutr. Soil Sci.* **163**, 433–439.

Levy-Booth D. J., Campbell R. G., Gulden R. H., Hart M. M., Powell J. R., Klironomos J. N., Pauls K. P., Swanton C. J., Trevors J. T. and Dunfield K. E. (2007) Cycling of DNA in the soil environment. *Soil Biol. Biochem.* **39**, 2977–2991.

Lilienfein J., Qualls R. G., Uselman S. M. and Bridgham S. D. (2004) Adsorption of dissolved organic carbon and nitrogen in soils of a weathering chronosequence. *Soil Sci. Soc. Am. J.* **68**, 292–305.

Maie N., Parish K. J., Watanabe A., Knicker H., Benner R., Abe T., Kaiser K. and Jaffé R. (2006) Chemical characteristics of dissolved organic nitrogen in an oligotrophic subtropical coastal ecosystem. *Geochim. Cosmochim. Acta* **70**, 4491–4506.

Matrajt G. and Blanot D. (2004) Properties of synthetic ferrihydrite as an amino acid adsorbent and a promoter of peptide bond formation. *Amino Acids* **26**, 153–158.

Mikutta R., Mikutta C., Kalbitz K., Scheel T., Kaiser K. and Jahn R. (2007) Biodegradation of forest floor organic matter bound to minerals via different binding mechanisms. *Geochim. Cosmochim. Acta* **71**, 2569–2590.

Mikutta R., Schaumann G., Gildemeister D., Bonneville S., Kramer M. G., Chorover J., Chadwick O. A. and Guggenberger G. (2009) Biogeochemistry of mineral–organic associations across a long-term mineralogical soil gradient (0.3–4100 kyr), Hawaiian Islands. *Geochim. Cosmochim. Acta* **73**, 2034–2060.

Moritz L. K., Liang C., Wagai R., Kitayama K. and Balser T. C. (2009) Vertical distribution of pools of microbial residues in tropical forest soils formed from distinct parent materials. *Biogeochemistry* **92**, 83–94.

Nguyen R. T. and Harvey H. R. (2001) Preservation of protein in marine systems: hydrophobic and other noncovalent associations as major stabilizing forces. *Geochim. Cosmochim. Acta* **65**, 1467–1480.

Omoike A. and Chorover J. (2006) Adsorption to goethite of extracellular polymeric substances from *Bacillus subtilis*. *Geochim. Cosmochim. Acta* **70**, 827–838.

Patience R. L., Baxby M., Bartle K. D., Perry D. L., Rees A. G. W. and Rowland S. J. (1992) The functionality of organic nitrogen in some recent sediments from the Peru upwelling region. *Org. Geochem.* **18**, 161–169.

Paul E. A. and Clark F. E. (1996) *Soil Microbiology and Biochemistry*. Academic Press, San Diego.

Paul S., Veldkamp E. and Flessa H. (2008) Differential response of mineral-associated organic matter in tropical soils formed in volcanic ashes and marine Tertiary sediment to treatment with HCl, NaOCl, and $Na_4P_2O_7$. *Soil Biol. Biochem.* **40**, 1846–1855.

Rafalska J., Engel M. H. and Lanier W. P. (1991) Retardation of racemization rates of amino acids incorporated into melanoidins. *Geochim. Cosmochim. Acta* **55**, 3369–3675.

Ressler T. (1998) WinXAS: a program for X-ray absorption spectroscopy data analysis under MS-Windows. *J. Synchroton Rad.* **5**, 118–122.

Rovira P. and Vallejo V. R. (2003) Physical protection and biochemical quality of organic matter in mediterranean calcareous forest soils: a density fractionation approach. *Soil Biol. Biochem.* **35**, 245–261.

Safari Sinegani A. A., Emtiazi G. and Shariatmadari H. (2005) Sorption and immobilization of cellulase on silicate clay minerals. *J. Colloid Interface Sci.* **290**, 39–44.

Scheel T., Haumaier L., Ellerbrock R. H., Rühlmann J. and Kalbitz K. (2008) Properties of organic matter precipitated from acidic forest soil solutions. *Org. Geochem.* **39**, 1439–1453.

Sollins P., Swanston C., Kleber M., Filley T., Kramer M., Crow S., Caldwell B. A., Lajtha K. and Bowden R. (2006) Organic C and N stabilization in a forest soil: evidence from sequential density fractionation. *Soil Biol. Biochem.* **38**, 3313–3324.

Somei M. and Yamada F. (2004) Simple indole alkaloids and those with a nonrearranged monoterpenoid unit. *Nat. Prod. Rep.* **21**, 278–311.

Stuiver M. and Polach H. A. (1977) Reporting of ^{14}C data. *Radiocarbon* **19**, 355–363.

Swanston C. W., Torn M. S., Hanson P. J., Southon J. R., Garten C. T., Hanlon E. M. and Ganio L. (2005) Initial characterization of processes of soil carbon stabilization using forest stand-level radiocarbon enrichment. *Geoderma* **128**, 52–62.

Vairavamurthy A. and Wang S. (2002) Organic nitrogen in geomacromolecules: insights on speciation and transformation with K-edge XANES spectroscopy. *Environ. Sci. Technol.* **36**, 3050–3056.

Van Hees P. A. W., Jones D. L., Finlay R., Godbold D. L. and Lundström U. S. (2005) The carbon we do not see—the impact of low molecular weight compounds on carbon dynamics and respiration in forest soils: a review. *Soil Biol. Biochem.* **37**, 1–13.

Veuger B., Middelburg J. J., Boschker H. T. S. and Houtekamer M. (2007) Update of "Analysis of ^{15}N incorporation into D-alanine: a new method for tracing nitrogen uptake by bacteria". *Limnol. Oceanogr.: Methods* **5**, 192–194.

Vitousek P. M. (2004) Nutrient cycling and limitation: Hawaii as a model system. Princeton University Press.

Yu Z., Zhang Q., Kraus T. E. C., Dahlgren R. A., Anastasio C. and Zasoski R. J. (2000) Contribution of amino compounds to dissolved organic matter in forest soils. *Biogeochemistry* **61**, 173–198.

Zang X., van Heemst J. D. H., Dria K. J. and Hatcher P. G. (2000) Encapsulation of protein in humic acid from a histosol as an explanation for the occurrence of organic nitrogen in soil and sediment. *Org. Geochem.* **31**, 679–695.

Zhang X., Amelung W., Yuang Y. and Zech W. (1998) Amino sugar signature of particle-size fractions in soils of the native prairie as affected by climate. *Soil Sci.* **163**, 220–229.

Zhang X. and Amelung W. (1996) Gas chromatographic determination of muramic acid, glucosamine, mannosamine, and galactosamine in soils. *Soil Biol. Biochem.* **28**, 1201–1206.

Associate editor: Jay A. Brandes